Identification of a novel, tunable interface in the *S.pombe* HP1 protein, Swi6, that underpins epigenetic inheritance.

Amanda Ames[1], Melissa Seman[1,5], Ajay Larkin[1,5], Gulzhan Raiymbek[2], Ziyuan Chen[4], Alex Levashkevich[1], Julie Suzanne Biteen[3,4], and Kaushik Ragunathan[1*]

[1] Department of Biology, Brandeis University, Waltham, MA 02453

[2] Department of Biological Chemistry, University of Michigan, Ann Arbor, MI 48109

[3] Department of Chemistry, University of Michigan, Ann Arbor, MI 48104

[4] Department of Biophysics, University of Michigan, Ann Arbor, MI 48104

[5] These authors contributed equally.

* Correspondence: kaushikr@brandeis.edu (K.R.)

ABSTRACT

HP1 proteins bind dynamically to H3K9 methylation and are essential for establishing and maintaining transcriptionally silent epigenetic states, known as heterochromatin. HP1 proteins can dimerize, forming a binding interface that interacts with and recruits diverse chromatin-associated factors. HP1 proteins rapidly evolve through sequence changes and gene duplications, but the extent of variation required to achieve functional specialization is unknown. To investigate how changes in amino acid sequence impact epigenetic inheritance, we performed a targeted mutagenesis screen of the dimerization and protein interaction domain of the *S.pombe* HP1 homolog Swi6. We discovered that substitutions mapping to an auxiliary motif in Swi6 outside the dimerization interface can lead to complete functional divergence. Specifically, we identified point mutations at a single amino acid residue that resulted in either persistent gain or loss of function in epigenetic inheritance without affecting heterochromatin establishment. These substitutions increase Swi6 chromatin occupancy *in vivo* and alter Swi6-protein interactions that selectively affect H3K9me inheritance. Based on our findings, we propose that relatively minor changes in Swi6 amino acid composition can lead to profound changes in epigenetic inheritance, underscoring the remarkable plasticity associated with HP1 proteins and their ability to evolve new functions.

INTRODUCTION

Chromatin organization is critical for maintaining genome integrity and regulating gene expression (Misteli, 2020). Establishing distinct chromatin compartments consisting of active or repressed genes depends, in part, on the post-translational modifications of DNA packaging proteins called histones (Allfrey et al., 1964; Hildebrand and Dekker, 2020; Rea et al., 2000). Inheriting chromatin states following DNA replication enables cells to maintain their unique identities (Reinberg and Vales, 2018; Ringrose et al., 2004). Disrupting the epigenetic regulatory landscape leads to aneuploidy and genome instability, which are established hallmarks of cancer (Hanahan and Weinberg, 2011). Over 50% of all sequenced cancers have at least a single mutation in core histones, histone-binding proteins, or nucleosome remodelers, underscoring the devastating impacts of epigenetic misregulation in cancer (Flavahan et al., 2017). Therefore, advancing our knowledge of how epigenetic states are established and maintained is critical to illuminate normal cellular physiology and potentially develop novel, innovative therapeutic strategies.

Site-specific DNA or RNA binding proteins recruit histone modifiers to target unique locations in the genome to place repressive histone modifications as part of a process referred to as "*establishment* (Moazed, 2011). These repressive modifications can then be propagated over multiple cell divisions in a DNA sequence-independent manner through a process known as "*maintenance"* or *"epigenetic inheritance"*. The molecular basis for epigenetic inheritance is thought to involve the random but equal partitioning of modified H3-H4 parental histones between daughter DNA strands during each cycle of DNA replication (Petryk et al., 2018; Xu et al., 2010; Yu et al., 2018). In this model, modified histones are expected to serve as templates to restore pre-existing histone modification states on newly synthesized DNA (Stewart-Morgan et al., 2020). However, studies demonstrating the critical roles of non-histone proteins in regulating epigenetic inheritance challenge this traditional model, which is based solely on the partitioning of modified parental histones. For example, *in vitro* reconstitution studies show that

PRC1 (polycomb repressive complex 1), a protein complex that belongs to the Polycomb group (PcG) and is involved in H3K27 (histone 3 lysine 27) methylation (H3K27me) dependent silencing, remains continuously bound to old and newly replicated DNA independent of H3K27me (Francis, 2009). Furthermore, the ability of PRC1 to undergo liquid-liquid phase separation and form condensates in conjunction with modified histones can tune epigenetic memory (Eeftens et al., 2021). In an analogous silencing pathway, proteins called Heterochromatin Protein 1 (HP1) recognize and bind to histone 3 lysine 9 (H3K9) methylation (H3K9me), remain bound to their cognate chromatin marks both before and after DNA replication, suggesting that HP1 proteins might be part of the epigenetic imprint (Nakayama, 2000). HP1 proteins can also undergo phase separation, and their ability to oligomerize is crucial for maintaining epigenetic memory (Seman et al., 2023). Collectively, these results suggest that proteins that can drive changes in chromatin organization may precede or act in parallel with the inheritance of modified chromatin states. However, the mechanisms that coordinate the interplay between histone and non-histone proteins to enable epigenetic inheritance remain poorly understood.

Reader domains that recognize and bind to specific histone modifications play important roles in specifying the transcriptional context of an epigenetic state (Strahl and Allis, 2000). Canonical reader domains, such as bromodomains, chromodomains, and Tudor domains, are part of protein complexes that moderate gene expression and chromatin accessibility (Yun et al., 2011). Intriguingly, some reader domain paralogs bind to the same mark yet produce opposite transcriptional outcomes (Vakoc et al., 2005). Many regulatory mechanisms contribute to this diversity, including multivalent interactions with nucleosomes, RNA or DNA, autoinhibition driving protein conformational changes, and cooperative binding to combinations of histone modifications (Canzio et al., 2014; Lu and Wang, 2013; Sanchez and Zhou, 2011). Readers are enigmatic because, despite being highly conserved, their ability to be co-opted by diverse effectors enables them to fulfill functionally distinct roles in regulating gene expression (Franklin

et al., 2022). By co-opting reader domains, histone-modifying enzymes can engage in a process called 'read-write' wherein pre-existing histone modifications can recruit enzymes to modify newly incorporated histones (Audergon et al., 2015; Brickner, 2023; Ragunathan et al., 2015; Uckelmann and Davidovich, 2021; Zhang et al., 2008a). These observations underscore the indispensable role of reader domains in promoting epigenetic inheritance.

A pivotal reader domain-containing protein involved in heterochromatin formation is heterochromatin protein 1 (HP1) (James and Elgin, 2023). HP1 proteins have both a conserved chromodomain (CD), which binds specifically to H3K9me, and a chromoshadow domain (CSD) that promotes dimerization (Bannister et al., 2001; Cowieson et al., 2000). HP1 proteins can engage in higher-order interactions, leading to the formation of condensates that have liquid-like or gel-like properties *in vitro* and *in vivo* (Larson et al., 2017; Sanulli et al., 2019; Strom et al., 2017; Yamada et al., 1999). Although its physiological relevance remains an active area of investigation, one possibility is that the ability of HP1 proteins to form condensates leads to the assembly of distinct compartments that increase the local concentrations of silencing factors while selectively excluding transcriptional activators (Larson and Narlikar, 2018; Zhang et al., 2023). Upon dimerization, the CSD subunits also create a binding interface that facilitates protein interactions (Smothers and Henikoff, 2000). HP1s typically bind to proteins containing variations of a consensus pentapeptide motif, with the defining feature in most cases being a central valine residue, such as the PxVxL motif in mouse CAF1 or the LxVxI motif present in the *Drosophila* HP2 protein (Stephens et al., 2005; Thiru et al., 2004). Some HP1 variants demonstrate altered specificity for binding partners that contain degenerate equivalents of this motif. Notably, the *S.pombe* HP1 paralog Chp2 binds to a chromatin remodeler Mit1 through a CkIvV motif (Leopold et al., 2019). HP1 proteins recruit factors that both enhance and antagonize heterochromatin formation, many of which bind to the same shared CSD interface (Iglesias et al., 2020; Liu et al., 2017). This raises an important question about how the

recruitment of factors with opposing activities is coordinated, given that all these effectors presumably compete for the same CSD interface.

HP1 proteins are among the most rapidly evolving protein families (Helleu and Levine, 2018; Levine et al., 2012). An acute instance of this evolutionary dynamic is seen in Dipteran flies (Helleu and Levine, 2018). Phylogenomic studies reveal an unusually high number of HP1 gene duplications, leading to new opportunities for functional specialization of paralogs. These young HP1 genes show an elevated percent identity at amino acid positions involved in histone modification recognition and protein dimerization, indicating they are functional HP1 paralogs that evolved through positive selection (Helleu and Levine, 2018). In contrast, across HP1 paralogs, and to a more considerable extent between HP1 orthologs, there is substantial variation in amino acid residues at positions within the CD and CSD that are functionally undefined (Canzio *et al.*, 2014; Thiru *et al.*, 2004). Non-conserved sequences could contribute to functional diversity in HP1 proteins by influencing some paralog-specific functions. In mouse HP1a, the N-terminal extension serves as a site for hyperphosphorylation, which leads to higher chromatin binding and compaction (Hiragami-Hamada et al., 2011). The strength of CSD dimerization, which can be influenced by amino acid composition in the CSD and C-terminal extension, can differ across HP1 proteins and is thought to tune their affinity for various protein ligands further (Canzio *et al.*, 2014; Mendez et al., 2011; Mendez et al., 2013). However, we have limited knowledge of how much sequence variation is required to alter the function of HP1 proteins and achieve specialization.

The fission yeast *Schizosacchromyces pombe* (*S.pombe*) represents a minimal system to study heterochromatin (Allshire and Ekwall, 2015). Heterochromatin establishment and maintenance involves H3K9 methylation and the enzymatic activity of an H3K9 methyltransferase in *S.pombe* called Clr4, a Suv39h homolog (Ivanova et al., 1998). *S.pombe* has two HP1 reader proteins, Chp2 and Swi6, with extensive sequence similarity and shared structural similarities to HP1 proteins in metazoans, including an H3K9me binding

chromodomain (CD) and a dimerization domain (CSD) (Isaac et al., 2017; Sadaie et al., 2008; Thon and Verhein-Hansen, 2000). Swi6 and Chp2 have distinct yet additive roles in transcriptional silencing at pericentromeric repeats, telomeres, and the mating type locus (Motamedi et al., 2008). The two HP1 proteins interact with distinct sets of heterochromatin regulators and have vastly different expression levels (Swi6 is expressed 100-fold higher than Chp2) (Sadaie et al., 2023). Swi6 interacts with many factors, including those involved in RNAi-mediated heterochromatin formation, the histone deacetylase (Clr3), and a putative H3K9 demethylase (Epe1) (Fischer et al., 2009; Hayashi et al., 2012; Iglesias *et al.*, 2020; Raiymbek et al., 2020; Rougemaille et al., 2012; Yamada et al., 2005; Zofall and Grewal, 2006). Chp2 recruits the Snf2/HDAC repressive effector complex (SHREC) that includes Clr3 and the chromatin remodeler Mit1 to promote transcriptional silencing (Leopold *et al.*, 2019; Motamedi *et al.*, 2008; Ragunathan *et al.*, 2015).

Given the potential role of reader proteins, such as Swi6, in epigenetic inheritance, we anticipated that their plasticity to evolve new protein-protein interactions could serve as a potential mechanism to tune epigenetic memory. To determine how sequence changes in Swi6 can alter epigenetic inheritance, we performed a targeted PCR-based mutagenesis screen. By modifying the amino acid composition in the Swi6-CSD through a targeted, PCR-based mutagenesis strategy, we completely changed the durability of H3K9me-dependent epigenetic inheritance. Notably, we identified point mutations at a single residue (Thr 278) that are sufficient to achieve complete functional divergence. While some amino acid substitutions at this residue produced a gain of function maintenance phenotype, other substitutions at the same site resulted in a persistent loss of function phenotype. Furthermore, we determined that a gain of function substitution led to specific alterations in protein-protein interactions that are known to regulate epigenetic inheritance, including a loss of interaction with the putative H3K9 demethylase Epe1 and a gain of interaction with proteins involved in ribosome biogenesis. Additionally, these substitutions altered Swi6 chromatin occupancy *in vivo*. Our study reveals

that an HP1 protein, and possibly other reader proteins alike, can display substantial plasticity wherein relatively minor variations in amino acid composition outside primary structural interfaces can produce strikingly different functional outcomes.

RESULTS

A targeted mutagenesis screen identifies new Swi6 variants associated with a single amino acid position that affects epigenetic inheritance.

To uncouple the effects of sequence-dependent heterochromatin establishment from epigenetic inheritance, we used a system where a TetR-Clr4-I fusion protein binds to *10X-tetO* DNA binding sequences placed upstream of an *ade6+* reporter gene. TetR-Clr4-I binding allows for site-specific H3K9me deposition, leading to H3K9me establishment and *ade6+* silencing (Allshire et al., 1994; Audergon *et al.*, 2015; Ragunathan *et al.*, 2015). Cells appear red on low adenine media when *ade6+* is silenced and white when *ade6+* is expressed. The addition of tetracycline (+tet) triggers the release of TetR-Clr4-I, after which we can measure epigenetic inheritance without continuous initiation (**Figure 1A**). Consistent with previous work, deleting the eraser of H3K9me, Epe1 (*epe1Δ)*, is necessary to maintain *ade6+* silencing, as indicated by the appearance of red and sectored colonies that persist on +tetracycline-containing medium in contrast to white colonies in *epe1+* cells (**Figure 1B**, *epe1+* versus *epe1Δ,* +tet).

To determine the role of Swi6 in epigenetic inheritance, we generated a site-directed mutagenesis library using tiling primers containing degenerate NNN codons for each amino acid position. Since it is the primary interaction site for heterochromatin-associated factors, we focused our mutagenesis efforts on the Swi6-CSD, consisting of 65 amino acids. This PCR-based *swi6-CSD* variant library was integrated into the *S.pombe* genome to replace the endogenous *swi6+* sequence (**Supplemental Figure 1A**). To identify Swi6 gain-of-function mutations that lead to enhanced maintenance, we transformed our *swi6*-CSD variant library in an *epe1+* background where cells are normally white when plated on +tet medium. We expected a gain-of-function Swi6 variant to produce red/sectored colonies on +tet medium.

Based on an initial hit in our screen (T278Y), we discovered that several Thr 278 substitutions produced a gain-of-function maintenance phenotype, including phenylalanine (F), tyrosine (Y), alanine (A), cysteine (C), and serine (S) (**Figure 1B**). This subset of residues are all conserved or semi-conserved substitutions with uncharged side chains (A, C, F, S, Y). When Thr 278 was replaced with amino acid substitutions containing charged side chains- we observed a gain of maintenance in the case of glutamate (E) and arginine (R) substitutions, but unexpectedly, we observed a loss of maintenance in the case of aspartate (D) and lysine (K) substitutions (**Figure 1C**). These phenotypic differences were not due to changes in Swi6 protein levels, given that the expression of all Thr 278 variants is comparable to Swi6-WT protein (**Supplemental Figure 1B**).

We quantitatively measured transcriptional silencing of the reporter locus in *swi6* T278Y (*swi6*-Y*)* and *swi6* T278K (*swi6*-K*)*. We performed quantitative real-time PCR (qRT-PCR) on the gene upstream of *10XTetO-ade6*, *SPCC330.06c*. Consistent with the *ade6+* silencing phenotype, *swi6*-Y*,* and *swi6*-K showed a similar decrease in RNA expression as observed in *swi6*-WT (**Figure 1D**). After 24 hours of growth in +tet, we observed the maintenance of reduced transcript levels in *swi6*-Y consistent with a gain of heterochromatin maintenance. Conversely*,* *swi6*-K cells showed increased transcript levels consistent with no heterochromatin maintenance (**Figure 1D**). We also measured H3K9me3 levels at *SPCC330.06c* using chromatin immunoprecipitation followed by qPCR (ChIP-qPCR) before and after adding tetracycline. As expected, we observed high H3K9me3 enrichment in the context of establishment (-tet) in both *swi6*-Y and *swi6*-K. In contrast, H3K9me3 persisted during maintenance (+tet) in the case of *swi6*-Y but not *swi6*-K (**Figure 1E**).

As mentioned previously, heterochromatin maintenance in our reporter system is critically dependent on the H3K9me eraser Epe1, with *epe1*Δ cells being the primary genetic context in which we observed red or sectored colonies on +tet media. To determine if the observed maintenance phenotypes in *swi6*-Y and *swi6*-K are dependent on Epe1, we deleted

Epe1 in both genetic backgrounds. We expected that *swi6*-Y gain-of-maintenance would either be unaffected or further enhanced by *epe1*Δ, whereas *swi6*-K would acquire a maintenance phenotype upon deleting *epe1*. Unexpectedly, maintenance was not restored in *swi6*–K *epe1*Δ cells, as indicated by the continued appearance of white colonies in +tet medium matching what we see in *swi6*-K *epe1+* cells. Although *epe1*Δ is sufficient to confer heterochromatin maintenance in *swi6*-WT cells, it fails to produce a maintenance phenotype in *swi6*-K expressing cells (**Figure 1F, Supplemental Figure 1C**). It is also noteworthy that *swi6*-Y *epe1*Δ cells exhibited a slightly weaker epigenetic maintenance phenotype with fewer sectored colonies than *swi6*-Y *epe1+* cells. Nevertheless, deleting *epe1*Δ in *swi6*-Y did not completely disrupt maintenance since we still observed persistent transcriptional silencing consistent with successful maintenance when cells were plated on +tet media (**Figure 1F, Supplemental Figure 1C**). Based on these findings, we concluded that *swi6*-Y has a persistent gain-of-function maintenance phenotype, whereas *swi6*-K, unlike *swi6*-WT, has a persistent loss-of-function maintenance phenotype.

One possibility is that Swi6 phosphorylation is affected by Thr 278 substitutions. We tested the effect of deleting Ckb1, a subunit of the casein kinase II complex (CK2) in *S.pombe* that phosphorylates Swi6. Ckb1-mediated phosphorylation leads to the disruption of heterochromatin silencing by inhibiting recruitment of the histone deacetylase Clr3 while concomitantly upregulating Epe1 occupancy at sites of heterochromatin formation (Shimada et al., 2009). Upon deleting the CK2 subunit, *ckb1* (*ckb1*Δ), *ade6+* silencing is lost in both *swi6*-WT and *epe1*Δ cells. Surprisingly, heterochromatin silencing remains intact in *ckb1*Δ *swi6*-Y cells, suggesting Swi6-Y gain-of-maintenance is not regulated by CK2 phosphorylation (**Figure 1G**).

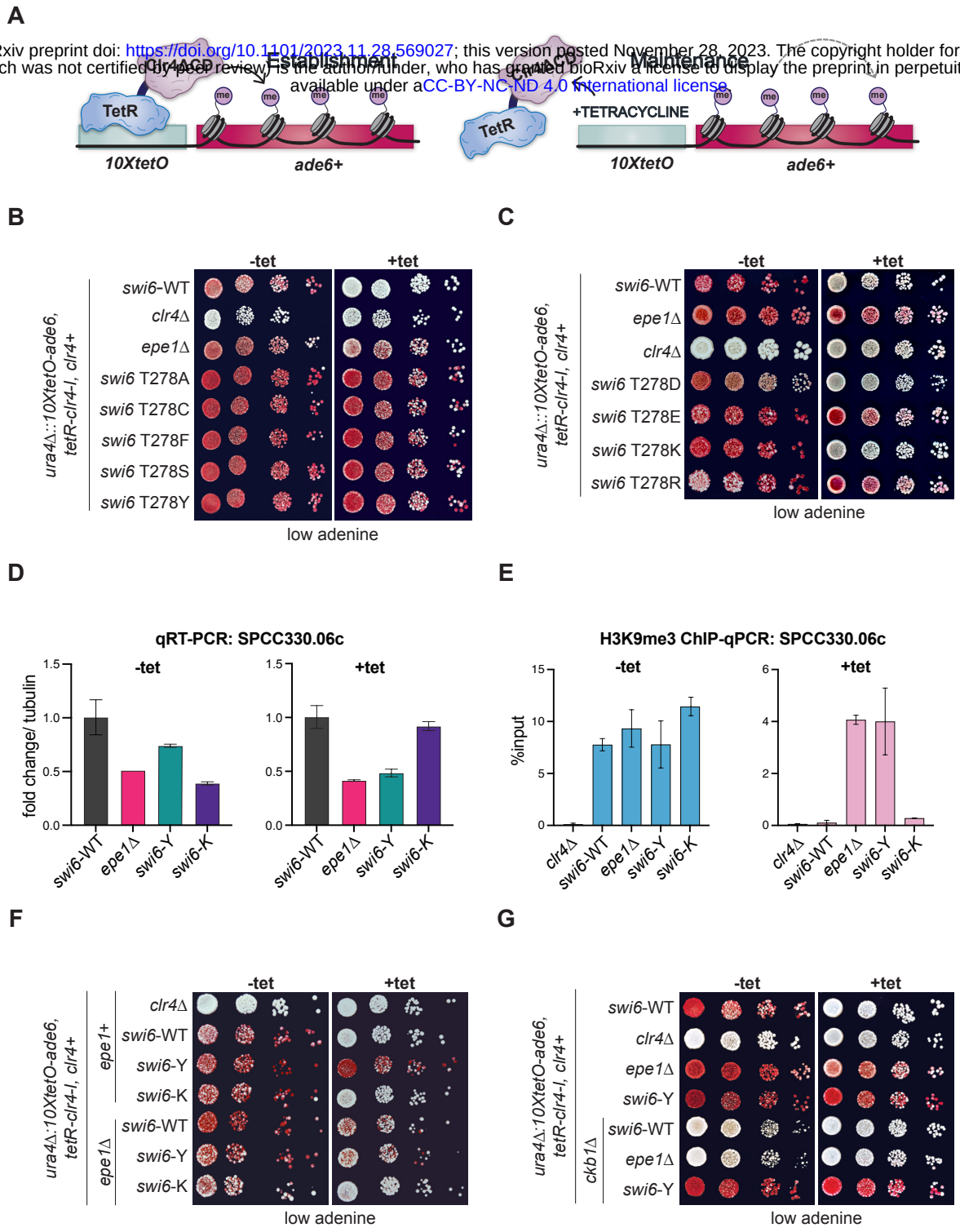

Figure 1. A targeted mutagenesis screen identifies new Swi6 variants associated with a single amino acid position that affects epigenetic inheritance. (A) Schematic of TetR-Clr4-I recruitment to 10XtetO binding sites upstream of an ade6+ reporter gene, initiating heterochromatin establishment. Addition of tetracycline (+tet) releases TetR-Clr4-I, enabling measurements of heterochromatin maintenance uncoupled from sequence-specific establishment. **(B-C)** Silencing assay of ura4Δ::10XtetO-ade6+ reporter in indicated genotypes in the absence (-tet) and presence (+tet) of tetracycline. Red cells indicate ade6+ silencing. Cells are plated as 10-fold serial dilutions. **(D)** qRT-PCR measuring RNA levels at SPCC330.06c in indicated genotypes before (-tet) and after (+tet) tetracycline addition. Error bars indicate SD (N = 2). **(E)** ChIP-qPCR measuring H3K9me3 at SPCC330.06c in indicated genotypes before (-tet) and after (+tet) tetracycline addition. Error bars indicate SD (N = 2). **(F-G)** Silencing assay of ura4Δ::10XtetO-ade6+ reporter in indicated genotypes in the absence (-tet) and presence (+tet) of tetracycline. Red cells indicate ade6+ silencing. Cells are plated at 10-fold serial dilutions.

Heterochromatin establishment and maintenance at endogenous and ectopic loci in Swi6 variants depends on H3K9 methylation.

To determine how *swi6*-Y or *swi6*-K substitutions affect heterochromatin spreading and its epigenetic inheritance, we performed chromatin immunoprecipitation followed by sequencing (ChIP-seq) of H3K9me2 and H3K9me3. We observed large H3K9me domains consistent with successful heterochromatin establishment proximal to the *10XtetO-ade6* reporter site across all Swi6 variant backgrounds (**Figure 2A-B**). Upon +tet treatment, H3K9me2 and H3K9me3 levels are maintained only in *swi6*-Y like what we observed in *epe1*Δ cells and completely lost in *swi6*-K like what we typically observe in *swi6*-WT (**Figure 2A-B**). These results suggest that the gain of maintenance phenotype we observed in *swi6*-Y is dependent on the inheritance of H3K9me.

To determine the extent to which both Swi6 variants affect constitutive heterochromatin, we replaced the endogenous *swi6*+ gene with *swi6*-Y and *swi6*-K in cells where an *ade6*+ reporter was inserted at the pericentromeric outer repeats (*otr1R(SphI)::ade6+)* (**Figure 2C**). Unlike *swi6*-WT cells that appeared uniformly red, we observed a small proportion of white, *ade6*+ expressing colonies in *swi6*-Y and *swi6*-K, suggesting a minor defect in pericentromeric reporter gene silencing. These minor silencing defects were also mirrored in our qRT-PCR analysis of pericentromeric (*dg* and *dh*) and telomeric (*tlh1*) transcripts (**Figure 2D**). Nevertheless, enrichment for H3K9me2 and H3K9me3 at pericentromeres were comparable in *swi6*-Y and *swi6*-K expressing cells (**Figure 2E, Supplemental Figure 2A-D**) while slightly decreased at telomeres in *swi6*-Y and *swi6*-K compared to *swi6*-WT cells. H3K9me2 and H3K9me3 levels at the rDNA locus were elevated in s*wi6*-Y but not in *swi6*-K, compared to *swi6*-WT (**Supplemental Figure 2A-D**). We also observed elevated H3K9me2 and H3K9me3 enrichment at facultative heterochromatin islands such as meiotic genes (*mei4* and *ssm4*) in *swi6*-K cells compared to *swi6*-WT (**Supplemental Figure 2E-F**).

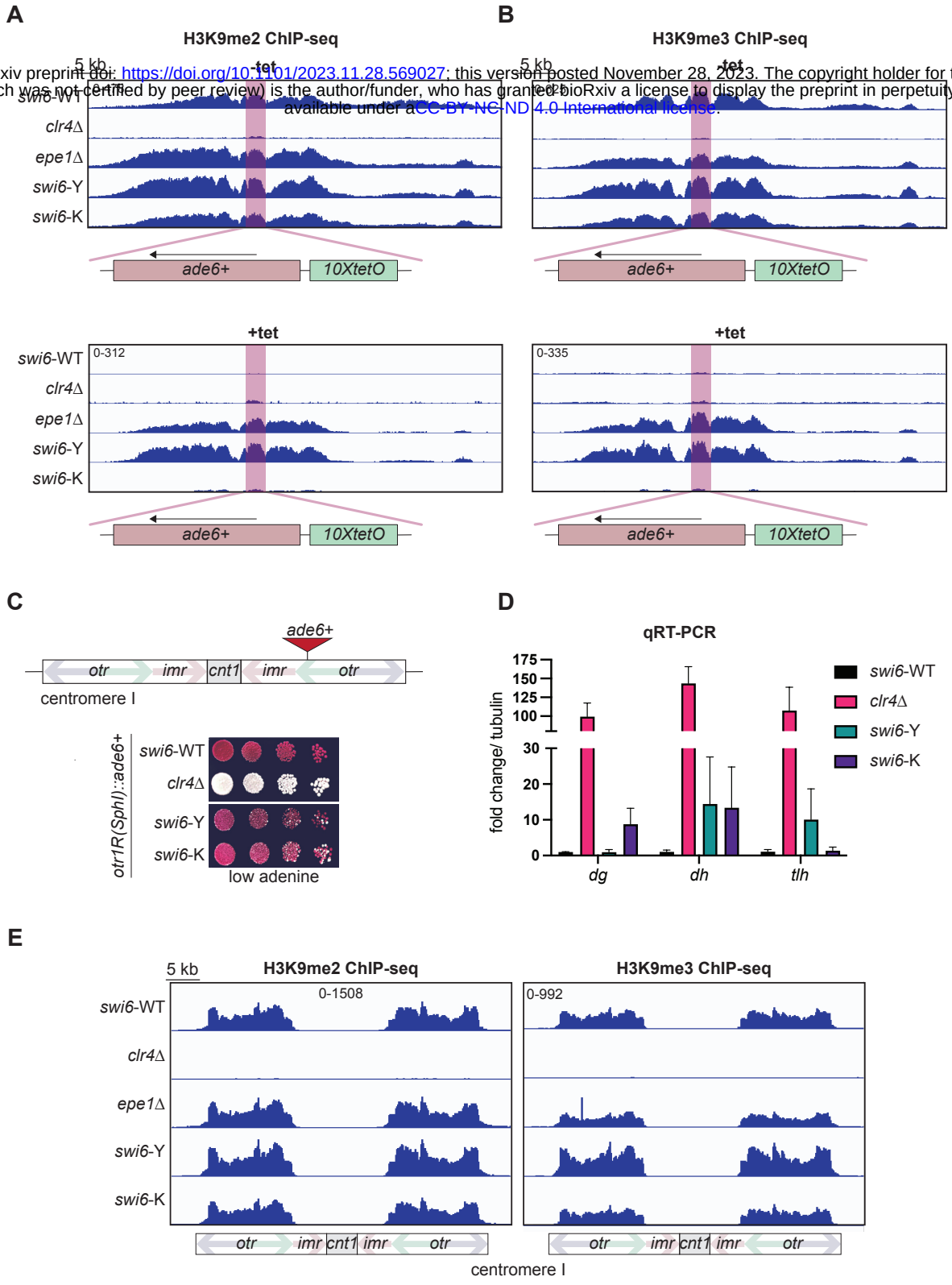

Figure 2. Heterochromatin establishment and maintenance at endogenous and ectopic loci in Swi6 variants depends on H3K9 methylation. (A-B) ChIP-seq of H3K9me2 **(A)** and H3K9me3 **(B)** surrounding the ura4Δ::10XtetO-ade6+ reporter in indicated genotypes and tetracycline treatment. The ura4Δ::10XtetO-ade6+ reporter is highlighted in red. Each ChIP-seq track corresponds to a 40kb region. Enrichment in all samples is shown as normalized reads per kilobase million (RPKM). **(C)** Top- Schematic detailing the otr1R::ade6+ reporter, where ade6+ is inserted within the outer pericentromeric repeats. Bottom- Silencing assay of otr1R::(SphI)ade6+ reporter in indicated genotypes. **(D)** qRT-PCR measuring RNA levels at dg, dh, and tlh in indicated genotypes and tetracycline treatment. Error bars indicate SD (N = 2). **(E)** ChIP-seq of H3K9me2 and H3K9me3 at the centromere on chromosome 1 in indicated genotypes. Each ChIP-seq track corresponds to a 45kb region with features within the centromere indicated in the schematic below. Enrichment in all samples is shown as normalized reads per kilobase million (RPKM).

Swi6-Y and Swi6-K variants disrupt a direct binding interaction with Epe1

As previously noted, deleting *epe1*Δ did not affect the maintenance phenotypes associated with Swi6-Y (gain-of-maintenance) or Swi6-K (loss-of-maintenance). We reasoned that our Thr 278 substitutions might disrupt a direct binding interaction between Epe1 and Swi6 while leaving other binding interactions required for heterochromatin establishment intact. We mapped the position of Thr 278 within the Swi6-CSD relative to the dimerization interface using an X-ray crystallography-based model (**Figure 3A**) (Cowieson *et al.*, 2000). The dimerization interface, consisting of two helices, facilitates hydrophobic contacts between two Swi6-CSD monomers via Leu 315. Disrupting the dimer by introducing a charged amino acid substitution (L315E or L315D) leads to a loss of silencing *in vivo* and a loss of H3K9me binding specificity *in vitro* (Canzio et al., 2011; Cowieson *et al.*, 2000). Interestingly, Thr 278 lies within a beta-sheet outside the dimerization interface, with its side chain being solvent-exposed. This observation supports our hypothesis that Thr 278 could be involved in tuning Swi6-dependent protein-protein interactions.

We generated strains expressing a C-terminal V5-tagged Epe1 (Epe1-V5) to detect the Swi6-Epe1 interaction using coimmunoprecipitation assays (CoIP) (**Figure 3B**). As expected, Swi6-WT copurifies with Epe1-V5 from cell lysates, consistent with the two proteins directly interacting *in vivo* (Raiymbek *et al.*, 2020). In contrast, Swi6 is no longer detected in Epe1-V5 purifications from cells expressing Swi6-Y or Swi6-K variants. This observation suggested that the Swi6-Epe1 interaction is disrupted in the case of both substitutions- Swi6-Y and Swi6-K irrespective of whether the mutants exhibit a gain of maintenance or a loss of maintenance phenotype (**Figure 1B-C**). To further confirm that altering Thr 278 had a direct effect on Epe1 binding, we performed a pulldown-based binding assay using recombinantly expressed and purified FLAG-Swi6 and MBP-Epe1 (**Supplemental Figure 3A**). Consistent with our coIP results, we detected an interaction between Epe1 and FLAG-Swi6-WT but not in the case of FLAG-Swi6-K *in vitro*. In fact, FLAG-Swi6-K abolished Epe1 binding to a similar extent as our

negative control FLAG-Swi6 L315E, a mutation known to completely disrupt Swi6 dimerization and all PxVxL-dependent protein interactions (Brasher et al., 2000; Haldar et al., 2011; Thiru *et al.*, 2004).

Consistent with our *ade6*+ establishment phenotypes and Epe1 binding observations, *swi6*-Y and *swi6*-K cells grown in -tet media also did not exhibit any additional enrichment of H3K9me2 and H3K9me3 in *epe1*Δ cells compared to *epe1*+ cells (**Figure 1F, 3C-D**). However, H3K9me2 and H3K9me3 enrichment is selectively observed only in *swi6*-Y *epe1*Δ but not *swi6*-K *epe1*Δ cells when grown in +tet media, which is fully consistent with their *ade6*+ maintenance phenotypes (**Figure 1F, 3C-D**).

To determine the molecular basis for how Swi6-Y or Swi6-K affects Epe1 binding, we used AlphaFold2 Multimer (AF-M) to generate a structural model of the interaction between Epe1 and Swi6 (Evans et al., 2022). First, we generated a structural prediction of the Swi6-CSD dimer. All five models predicted the dimer as expected, with the highest-ranking model aligning to the published crystal structures with an RMSD value of 0.49 Å (**Supplemental Figures 3B and 4**). Next, we generated a structural prediction of the Swi6-CSD dimer and Epe1ΔC (amino acids 1–600), which we previously showed is sufficient to strongly interact with Swi6 (**Supplemental Figure 3C**) (Raiymbek *et al.*, 2020). We generated five models, all confidently predicting that Epe1ΔC binds to the Swi6 dimerization interface via a PxVxL-like IGVVI motif (**Supplemental Figures 3C and 5**, residues 569-573). Consistent with most other variant HP1 interacting motifs, the key feature of this interaction sequence is the presence of a central valine residue. In addition to this primary mode of interaction, we observed a second interaction interface- namely, a predicted helix in Epe1 that interacts with the auxiliary Swi6 beta-sheet motif containing Thr 278. We deleted the region of Epe1 predicted to interact with the CSD dimer (residues 566-600) to generate a new allele of Epe1 (*epe1*Δ566-600), which harbors an internal deletion while the rest of the protein is intact. Consistent with a loss of interaction between Swi6 and Epe1, we observe an increase in red or sectored colonies when cells were

plated on +tet, consistent with increased heterochromatin maintenance much like what we previously observed in *epe1*Δ cells (**Supplemental Figure 3D,** *epe1*Δ566-600 *compared to epe1*+). To determine if the interaction with the auxiliary motif where Thr 278 is embedded is generalizable, we generated a structural prediction of the Swi6-CSD dimer and Sgo1, a known Swi6 interactor (**Supplemental Figures 3E and 6**) (Yamagishi et al., 2008). We observed similar interactions in the Sgo1-Swi6 predicted structure. A helix within Sgo1, distal to the PxVxL motif, interacts with the auxiliary Swi6 beta-sheet interface containing Thr 278. These predictions suggest that the beta-sheet within the Swi6 CSD could serve as a novel binding site outside of the dimerization interface that dictates Swi6 binding partner specificity.

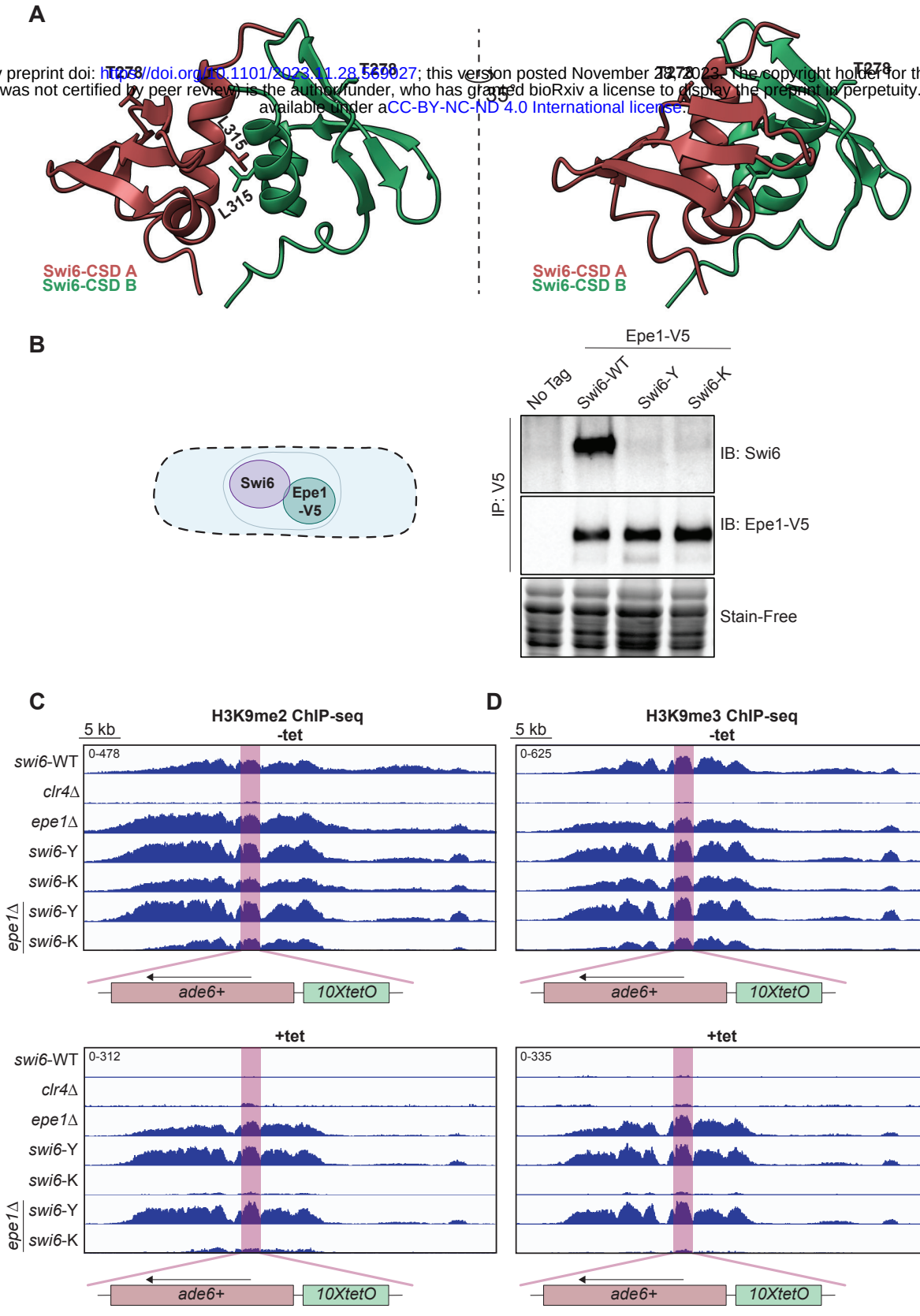

Figure 3. Swi6-Y and Swi6-K variants disrupt a direct binding interaction with Epe1. (A) X-ray crystallography structure of a Swi6-CSD dimer (PDB 1E0B, 1.90 Å). The dimerization interface and the side chains of Leu 315, a residue crucial for dimerization, are labeled. Thr 278 maps to a beta sheet interface with its side chain facing outward away from the dimerization interface. **(B)** Western blots of V5 coimmunoprecipitation (CoIP) performed with cell lysates to test the interaction between Epe1-V5 and Swi6. Epe1 is detected using a V5 antibody and Swi6 is detected using a primary antibody. **(C-D)** ChIP-seq of H3K9me2 **(C)** and H3K9me3 **(D)** surrounding the ura4Δ::10XtetO-ade6+ reporter in indicated genotypes and tetracycline treatment. The ura4Δ::10XtetO-ade6+ reporter is highlighted in red, displayed in a 40kb region. Enrichment in all samples is shown as normalized reads per kilobase million (RPKM).

Swi6-Y and Swi6-K mutations have no significant effect on nucleosome binding *in vitro* but exhibit increased chromatin *occupancy in vivo*

We considered whether the molecular basis for the divergence in phenotypes between Swi6-Y (gain of maintenance) and Swi6-K (loss of maintenance) might arise from biochemical differences such as Swi6 dimerization or nucleosome binding. We recombinantly expressed and purified different Swi6 variants (including Swi6-WT) from *E. coli* and analyzed their dimerization and nucleosome binding properties *in vitro* (**Figure 4A-C, Supplemental Figures 7 and 8**). We used mass photometry to measure the relative abundance of Swi6 species across a low nanomolar concentration range (2.5-20 nM). Mass Photometry (MP) is a single-molecule approach that uses light to detect the number and molar mass of unlabeled molecules in dilute samples and, given its measurement range, we expected to detect mass differences between Swi6 monomers, dimers, and oligomers (Asor and Kukura, 2022; Sadaie *et al.*, 2008). We detected two molecular species with the predicted masses for a Swi6 monomer (37 kDa) and a Swi6 dimer (74 kDa) in Swi6-WT, Swi6-Y, and Swi6-K (**Supplemental Figure 7A-E**). The dimer population (74kDa) was not detected in Swi6 L315E, a mutation that disrupts Swi6 dimerization (**Supplemental Figure 7C**). The observed monomer-to-dimer ratios were consistent with concentration-dependent dimer formation. We predominantly observed dimers at our lowest measured concentration (2.5 nM), with monomers accounting for roughly 20% of the population (**Supplemental Figure 7D**). We determined apparent dimerization constants using our observed relative abundance values (K_{dim}, **Supplemental Figure 7F**) (Soltermann et al., 2020). Consistent with previous work, Swi6-WT dimerizes with an apparent K_{dim} of 0.38 nM. We did not observe a significant change in dimerization affinity in Swi6-Y and Swi6-K, with apparent K_{dim} values being 0.27 nM and 0.20 nM, respectively. Although there may be modest differences in dimerization that fall outside the detection limits of mass photometry, our results suggest dimerization is not significantly impacted by introducing Swi6-Y or Swi6-K mutations *in vitro*.

To measure Swi6-nucleosome binding affinity and specificity, we performed electrophoretic mobility shift assays (EMSAs) using reconstituted H3K9me0 or H3K9me3 mononucleosomes (**Figure 4A-C, Supplemental Figure 8)**. We observed a shift of unbound nucleosomes to higher molecular weight species as Swi6 binds in a concentration-dependent manner. After fitting our concentration-dependent binding assays, we determined that Swi6-WT binds to H3K9me3 mononucleosomes with an apparent K_d of ~50nM, which was very similar to the K_d for Swi6-Y binding to H3K9me3 nucleosomes (~39nM). In addition, both Swi6-WT and Swi6-Y bind to H3K9me3 mononucleosomes with similar specificity (2.4-fold for Swi6-WT and 2.3-fold for Swi6-Y) (**Figure 4A-C**). Consistent with previous studies, we confirmed the complete loss of specificity for H3K9me3 binding in control experiments measuring Swi6 L315E (**Figure 4C**). We detected no substantive differences between Swi6-WT and Swi6-Y in our *in vitro* nucleosome binding assays.

In vitro binding assays using mononucleosomes do not accurately reflect how Swi6 binds to chromatin *in vivo*, likely due to differences in substrate length and complexity (Biswas et al., 2022; Canzio *et al.*, 2011). To determine how Swi6-Y and Swi6-K bind to H3K9me in a native chromatin context, we mapped the dynamics of individual Swi6 molecules in living cells (**Figure 4D**) (Biswas *et al.*, 2022). We tracked PAmCherry-Swi6-Y and PAmCherry-Swi6-K dynamics and compared them to the dynamics of PAmCherry-Swi6-WT. For each mutant, we identified mobility states that best described the single-molecule trajectories we measured. Each state has a defined population and an average diffusion coefficient (**Figure 4E-F**) (Biswas *et al.*, 2022; Karslake et al., 2021). Swi6-WT has four mobility states, namely a fast-diffusing state (unbound Swi6), a medium-diffusing state (nucleic acid-associated Swi6), a slow-diffusing state (unmethylated H3K9 chromatin-associated Swi6), and a slowest-diffusing state (H3K9me2/3 chromatin-bound Swi6). Swi6-Y and Swi6-K exhibited only three mobility states in contrast to the four states we typically observed in the case of Swi6-WT (**Figure 4E-F**). The most prominent change in our mobility state measurements was a 2-fold reduction in the fraction of Swi6

molecules across the two variants that occupy the fast-diffusing mobility state, corresponding to unbound Swi6. The medium-diffusing mobility state, corresponding to nucleic acid-associated Swi6, was at the limit of our analysis and detection methods and hence not observed in either Swi6-Y or Swi6-K mutants. Furthermore, the fraction of Swi6 molecules in the mobility states that correspond to H3K9me chromatin-binding increased, with an estimated shift from 50% of Swi6-WT molecules being chromatin-bound to ~90% of Swi6-Y and Swi6-K molecules being chromatin-bound. We additionally analyzed our data using a posterior distribution analysis (DPSP) to avoid overfitting biases that may arise from Bayesian methods (Heckert et al., 2022). The posterior distribution analysis with DPSP revealed a greater proportion of molecules in low-mobility states (chromatin-bound) with a concomitant decrease in highly mobile (free) molecules in Swi6-Y and Swi6-K compared to Swi6-WT (**Figure 4G**). The DPSP analysis supports our findings of an increase in the number of trajectories corresponding to low mobility molecules in Swi6-Y and Swi6-K compared to Swi6-WT. Since Swi6-Y and Swi6-K have divergent maintenance phenotypes, our results suggested that mechanisms other than increased chromatin occupancy must contribute to the unusual maintenance phenotypes we observed.

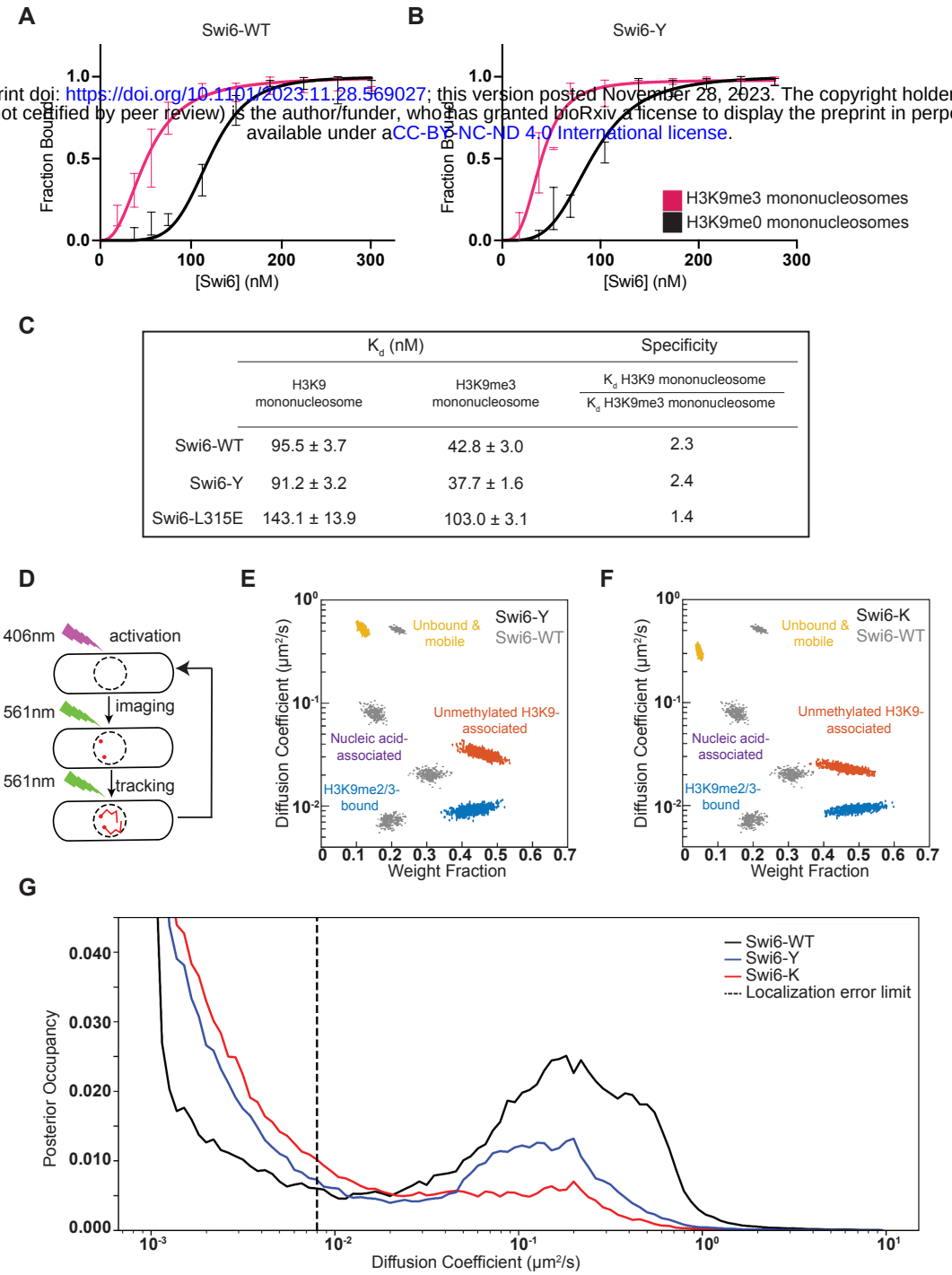

	K_d (nM)		Specificity
	H3K9 mononucleosome	H3K9me3 mononucleosome	$\frac{K_d \text{ H3K9 mononucleosome}}{K_d \text{ H3K9me3 mononucleosome}}$
Swi6-WT	95.5 ± 3.7	42.8 ± 3.0	2.3
Swi6-Y	91.2 ± 3.2	37.7 ± 1.6	2.4
Swi6-L315E	143.1 ± 13.9	103.0 ± 3.1	1.4

Figure 4. Swi6-Y and Swi6-K mutations have no significant effect on nucleosome binding in vitro but exhibit increased chromatin occupancy in vivo. (A-B) Concentration dependence curves of quantified electrophoretic mobility shift assays (EMSA) using H3K9me0 (black) and H3K9me3 (pink) mononucleosomes in **(A)** Swi6-WT and **(B)** Swi6-Y. Error bars indicate SD (N=5). **(C)** Table summarizing the apparent binding affinity (Kd) and specificity values observed for Swi6-WT, Swi6-Y and Swi6-L315E. **(D)** Schematic depicting single-molecule microscopy live-cell tracking workflow. PAmCherry-Swi6 molecules are photoactivated (406 nm) then imaged and tracked until photobleaching (561 nm, 25 frames/sec). The cycle is repeated 10 – 20 times/cell. **(E-F)** Mobility states detected by SMAUG analysis for **(E)** PAmCherry-Swi6-Y and **(F)** PAmCherry-Swi6-K. Each point is the average single-molecule diffusion coefficient of Swi6 following a single iteration of the Bayesian algorithm after convergence. Mobility states are color-coded by fast diffusing unbound state (yellow), moderately diffusing nucleic acid-associated state (purple), slow diffusing unmethylated H3K9 bound state (red), and slow diffusing H3K9me2/3 bound state (blue). Dataset: 17150 single-molecule steps from 2039 PAmCherry-Swi6-Y trajectories and 67 cells. 19718 single-molecule steps from 1225 PAmCherry-Swi6-K trajectories and 68 cells. Mobility states determined in Swi6-WT (gray) are plotted as a reference. **(G)** Posterior occupancy across diffusion coefficients for PAmCherry-Swi6-WT (black), Swi6-Y (blue), and Swi6-K (red) with DPSP analysis (Heckert et al, 2022). The dashed line represents the localization error limit separating fast diffusing molecules (right) from slow diffusing molecules (left).

A trade-off in protein-protein interactions between Epe1 and the rixosome with Swi6 promotes epigenetic inheritance.

Since the loss of Epe1 binding alone cannot explain the differential maintenance phenotypes we observed in Swi6-Y and Swi6-K, we investigated how all possible Swi6-dependent protein interactions are affected across the two variants using quantitative mass spectrometry (Iglesias *et al.*, 2020; Zhang and Elias, 2017). We generated N-terminal FLAG-Swi6 strains to perform tandem mass tag affinity purification mass spectroscopy (TMT-AP-MS, **Supplemental Figure 9A**). We compared protein interactions that were significantly altered in Swi6-Y and Swi6-K relative to Swi6-WT (**Figure 5A-B**). In agreement with our coIP measurements, Epe1 and its known binding partner Bdf2 are downregulated ~6-fold in Swi6-Y and Swi6-K (**Figure 5A-C**) (Wang et al., 2013). We also observed selective and significant upregulation of factors with known roles in ribosomal RNA (rRNA) processing, ribosome biogenesis, or nucleolar localization (~50% of all upregulated interactions) in the case of Swi6-Y but not Swi6-K. Among this group are the core subunits of the conserved rRNA processing and RNA degradation complex, the rixosome (**Figure 5A, C**) (Holla et al., 2020; Shipkovenska et al., 2020). We also noted a significant differential association of factors belonging to GO term categories, which included heterochromatin regulation, RNA polymerase II-mediated transcription, chromatin remodeling, RNA processing, DNA damage/cell cycle, and DNA replication (**Figure 5C-D**). We did not observe any significant changes in interactions with heterochromatin-associated factors that have known functions in epigenetic inheritance, which include subunits of the H3K9 methyltransferase CLRC complex, a deacetylase-remodeler complex, SHREC, the histone chaperone complex. FACT, nuclear pore complex subunits, and the nucleosome remodeler, Ino80 complex across both Swi6 variants (**Supplemental Figure 9B**) (Hirano et al., 2020; Holla *et al.*, 2020; Iglesias *et al.*, 2020; Shan et al., 2020; Takahata et al., 2021; Zofall, 2022).

Our quantitative mass spectrometry results suggested that the gain-of-maintenance phenotype we observed in Swi6-Y was determined by the extent of its interaction with subunits of the rixosome complex. To test this hypothesis, we generated a separation-of-function mutation in the Grc3 subunit of the rixosome (*grc3* V70M). This mutation disrupts the rixosome-Swi6 interaction without affecting its ribosome biogenesis functions (Shipkovenska *et al.*, 2020). *swi6*-Y *grc3* V70M exhibited red colonies in -tet media, consistent with successful heterochromatin establishment. However, cells plated on +tet media turned white, consistent with a loss of *ade6*+ silencing and selective disruption of maintenance (**Figure 5E**). Therefore, the enhanced maintenance phenotype in the case of Swi6-Y is critically dependent on its specific interaction with the rixosome complex.

We generated a model of the Swi6-CSD dimer and Grc3 using AF-M (**Supplemental Figure 9C**). Grc3 interacts with the Swi6-CSD dimer using a PxVxL-like motif, but the upstream and downstream contacts between Grc3 and the Swi6-CSD are strikingly different compared to what we previously observed in the case of Sgo1 and Epe1 (**Supplemental Figure 3C, F**). The helix that we previously noted in our Epe1-Swi6 and Sgo1-Swi6 structural models interacting with the Swi6 auxiliary motif containing Thr 278 was notably absent in all five Grc3-Swi6 models (**Supplemental Figure 10**). These *in silico* differences across Swi6 binding partners (Grc3, Sgo1, and Epe1) could provide a potential molecular basis for tunability that depends on interactions with an auxiliary binding motif that extends beyond the dimerization interface.

Site-specific HDAC recruitment does not bypass the requirement for the rixosome in heterochromatin maintenance.

Previous work has shown that targeting the histone deacetylase Clr3 to heterochromatin (either by tethering Clr3 or by fusing chromodomains) is sufficient for epigenetic inheritance despite the presence of Epe1 (Raiymbek *et al.*, 2020; Zofall, 2022). The HDAC activity of Clr3 reduces histone turnover, a characteristic feature of heterochromatin that is thought to promote epigenetic inheritance (Aygun et al., 2013). We wanted to test if tethering Clr3 is sufficient to

rescue defective maintenance in *grc3* V70M expressing cells. We expressed a Gal4 -Clr3 fusion protein in strains containing two orthogonal DNA binding sequences, i.e. *10XUAS* sites for Gal4 binding and *10XtetO* sites for TetR binding- both of which are placed upstream of the *ade6+* reporter gene (**Figure 5F**). Despite Epe1 being present, we observed robust maintenance of *ade6+* silencing, with cells appearing red or sectored when plated on +tet media (**Figure 5F**, *swi6*-WT*, gal4-clr3*). This process is critically dependent on Swi6 since both establishment and maintenance were eliminated in cells lacking Swi6 (**Figure 5F**, *swi6*Δ, *gal4-clr3*). Furthermore, targeting Clr3 could not bypass the requirement for the rixosome interaction in heterochromatin maintenance. In cells expressing *grc3*-V70M, tethering Clr3 failed to produce red or sectored colonies when cells were plated on +tet-containing medium (**Figure 5F**). These results support a model wherein the rixosome acts downstream of Clr3-mediated histone deacetylation during heterochromatin maintenance. Interestingly, tethering Clr3 only partially rescued the Swi6-K maintenance defect since we observed both successful establishment (red colonies, -tet) and maintenance (red or sectored colonies in +tet), although maintenance was not nearly as robust as what we observed in *swi6*-WT cells (**Figure 5F**). Hence, Clr3-mediated histone deacetylation can compensate for defective heterochromatin maintenance in the case of *swi6*-K but not in the case of *grc3*-V70M. These findings further implicate the rixosome as a critical factor in promoting epigenetic inheritance (Holla *et al.*, 2020; Shipkovenska *et al.*, 2020).

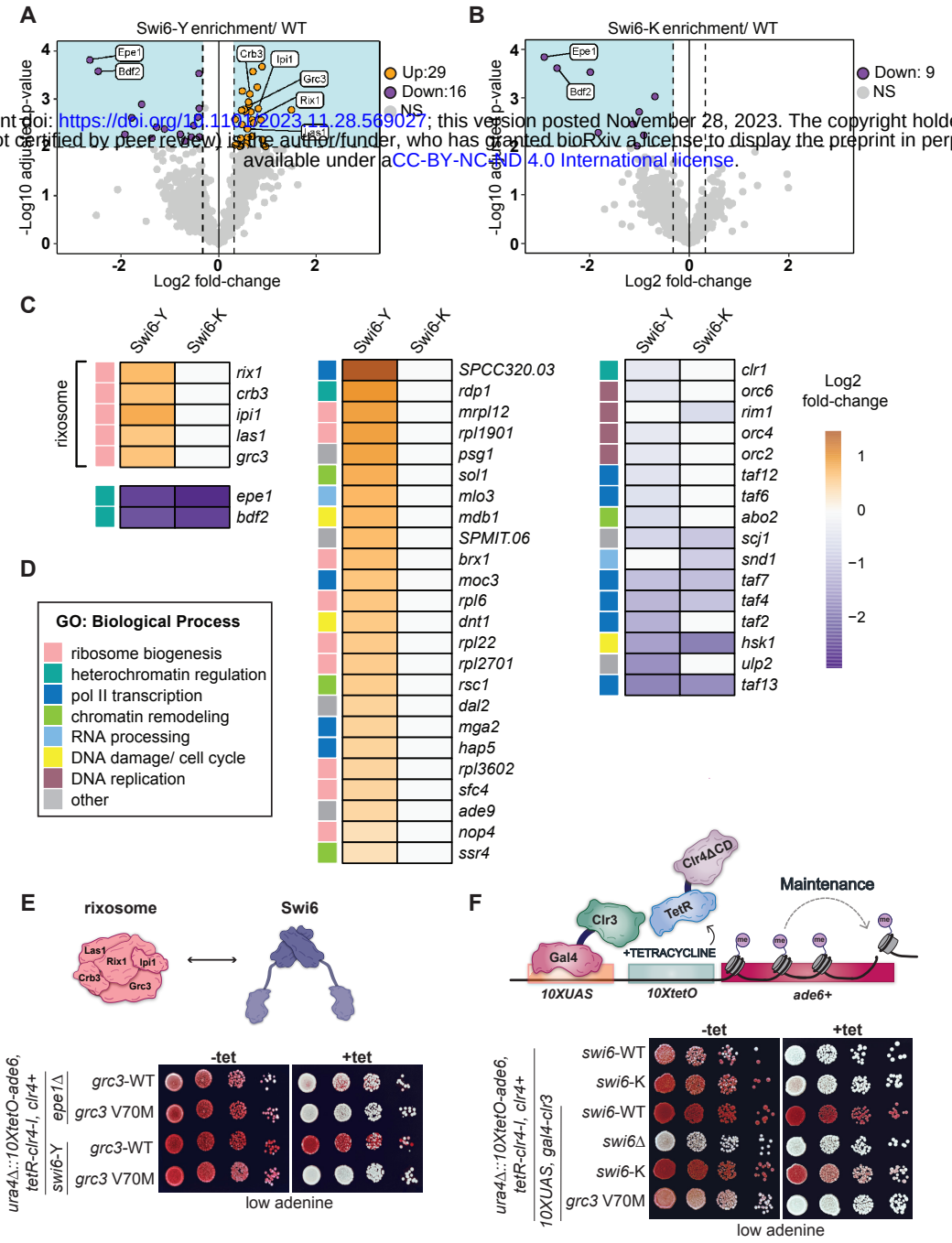

Figure 5. A trade-off in protein-protein interactions between Epe1 and the rixosome with Swi6 promotes epigenetic inheritance. (A-B) Volcano plot displaying the results from tandem mass tag mass spectrometry (TMT-MS) of affinity purifications of **(A)** 3XFLAG-Swi6-Y and **(B)** 3XFLAG-Swi6-K. Samples were normalized to untagged Swi6 and plotted against the reference (3XFLAG-Swi6-WT). The shaded boxes mark a p-value = 0.01 (horizontal) and a 1.25-fold enrichment over the 3XFLAG-Swi6-WT reference (vertical) (N = 3), only interactions detected with > 1 peptide are included in the dataset. Proteins are color-coded as upregulated interactions (orange), downregulated interactions (purple), unenriched interactions (grey), and relevant heterochromatin regulators are labeled. The full dataset of interacting proteins can be found in Supplementary Dataset 1. **(C)** Heat map comparing upregulated (orange) and downregulated (purple) interactions observed in Swi6-Y and Swi6-K, p-value cutoff is < 0.01. **(D)** GO term analysis of biological process categories for upregulated and downregulated interactions. Each interaction within the **(C)** heat map is annotated with a colored box, denoting its corresponding GO-term biological process. The sample size for each GO term is as follows: ribosome biogenesis N = 14, heterochromatin regulation N = 4, pol II transcription N = 10, chromatin remodeling N = 4, RNA processing N = 2, DNA damage/ cell cycle N = 3, DNA replication N = 4, other N = 6. **(E)** Top- Schematic of the rixosome complex subunits. Bottom- Silencing assay of ura4Δ::10XtetO-ade6+ reporter in indicated genotypes in the absence (-tet) and presence (+tet) of tetracycline. Red cells indicate ade6+ silencing. Cells are plated at 10-fold serial dilutions. **(F)** Top- schematic of the modified 10xUAS-10XtetO-ade6+ reporter system. The system contains ten copies of the UAS DNA binding sites placed upstream of 10XtetO. A Gal4-Clr3 fusion protein binds to these sites and remains bound in the presence of tetracycline. Bottom- silencing assay of ura4Δ::10xUAS-10XtetO-ade6+ reporter in indicated genotypes in the absence (-tet) and presence (+tet) of tetracycline. Red cells indicate ade6+ silencing. Cells are plated at 10-fold serial dilutions.

DISCUSSION

HP1 proteins have a conserved architecture yet are functionally versatile (Canzio *et al.*, 2014). We hypothesized that regions which exhibit high sequence variability within the otherwise conserved chromoshadow domain (CSD) could contribute towards HP1 proteins acquiring novel functional properties. To test this hypothesis, we used a targeted mutagenesis screen of the Swi6-CSD to identify new variants that exhibit enhanced heterochromatin maintenance. We have demonstrated that substitutions associated with a single amino-acid residue, Thr 278, within the Swi6-CSD can influence the maintenance of an ectopic heterochromatin domain while preserving Swi6 dimerization, nucleosome binding, and transcriptional silencing. Our findings support a model where sequence variation outside the dimerization interface can enable Swi6, and possibly other HP1 proteins, to acquire new functional attributes. Hence, the plasticity of HP1 proteins arises not from changes to conserved sites but from alterations within auxiliary regions that preserve overall protein architecture. *In silico* modeling of Epe1, Sgo1, and Grc3, with the Swi6-CSD dimer reveals minimal differences in how the PxVxL motif (or PxVxL variant motifs) bind to the Swi6-CSD dimer interface (Kang et al., 2011; Thiru *et al.*, 2004). In contrast, our predictions show significant divergence in motifs that may interact with the Thr 278-containing beta-sheet interface (**Supplemental Figures 3C, 3E, and 9C**). Although further validation is required to understand the structural implications of our generated models, our studies potentially reveal a new interface in an HP1 protein that determines protein binding specificity.

Although structural studies to support our AF-M models are currently unavailable, NMR measurements have identified interactions between peptides of Clr3, Sgo1, and histone H2B with the Swi6-CSD dimer (Isaac *et al.*, 2017; Sanulli *et al.*, 2019). These data also identified potential interactions involving Thr 278 and other neighboring residues within Swi6 (Isaac *et al.*, 2017; Sanulli *et al.*, 2019). Therefore, our experimental findings are consistent with a model where Thr 278 can function as a specificity determinant, thus enabling Swi6 to differentiate

between protein interactors, all of which share a PxVxL-like motif and bind to a common Swi6-CSD interface. The importance of Thr 278 in altering Swi6 function is also underscored by a screen for G0 suppressors, which previously identified Swi6 T278K (or Swi6-K) as a mutation that promotes the survival of fission yeast cells following quiescence (Roche et al., 2016). Hence, the interface we identified likely contributes to heterochromatin maintenance in G2 cells but may have other classes of interactors that depend on Swi6 during quiescence.

Previous studies identified HP1 mutations associated with the N-terminal chromodomain (CD) which affects H3K9me binding and oligomerization or the C-terminal chromoshadow domain (CSD) mutants that disrupt dimerization (Canzio *et al.*, 2011; Canzio et al., 2013; Jacobs and Khorasanizadeh, 2002; Jacobs et al., 2001; Thiru *et al.*, 2004; Yamagishi *et al.*, 2008). Since dimerization is crucial for HP1-dependent protein-protein interactions, it is nearly impossible to introduce mutations within the dimerization interface without compromising its overall structure and function. The variants we identified in our study map to an auxiliary motif outside the CSD dimerization interface. This enables selective tuning of protein-protein interactions without disrupting overall Swi6 function, especially in the context of heterochromatin establishment. While we have shown how the Epe1-rixosome-Swi6 axis is sensitive to substitutions within the auxiliary beta sheet binding interface, other studies have shown that the histone chaperone complex FACT, which directly binds to Swi6, is insensitive to mutations within this interface. In agreement with our proteomics data, Thr 278 substitutions (Swi6 T278K and T278A) do not alter the interaction between Swi6 and Spt16 (Takahata *et al.*, 2021). Furthermore, recent work has shown that the Drosophila HP1 protein Rhino utilizes its chromodomain to interact with the transcription factor Kipferl (Baumgartner et al., 2022). Moreover, mutations affecting Kipferl binding do not affect H3K9me recognition, suggesting this interface can also potentially be exploited for evolving new protein-protein interactions (Baumgartner et al., 2023).

We aligned HP1 sequences across the *Schizosaccharomyces* lineage (*S.cryophilus, S.japonicus, S.octosporus,* and *S.osmophilus*) and found minimal sequence variation within the auxiliary beta-sheet region across Swi6 orthologs (**Supplemental Figure 11**). However, sequence conservation within this region significantly declines when comparing Swi6 to Chp2 or HP1 proteins from other organisms (Mendez *et al.*, 2013; Thiru *et al.*, 2004). Hence, in addition to variations within PxVxL motif binding, we propose that the auxiliary beta sheet we identified can further contribute to functional divergence between HP1 proteins (Leopold *et al.*, 2019). The lineage and variant-specific conservation of this region have important consequences for envisioning what the "ground state" of heterochromatin systems might be in different organisms. Most substitutions, apart from the original Thr 278 residue, led to the persistent gain of epigenetic inheritance, and a subset of charged amino acid substitutions led to a persistent loss of epigenetic inheritance. Both extreme scenarios' consequences are absolute, with heterochromatin being inflexible and not regulatable. Therefore, our findings suggest Thr 278 and possibly the surrounding amino acids within the beta-sheet interface in Swi6 contribute to epigenetic plasticity wherein cells can invoke memory depending on changes in their physiology or environment.

Consistent with this model, there are proposed mechanisms for regulating Swi6 protein interactions that may contribute to epigenetic plasticity. Notably, heterochromatin maintenance in *S.pombe* is responsive to environmental changes, which can be regulated by altering Epe1 availability in cells. Epe1 expression is sensitive to glucose availability, cAMP levels, stress, and ubiquitination (Bao et al., 2022; Bao et al., 2019; Braun et al., 2011; Torres-Garcia et al., 2020b; Yaseen et al., 2022). Furthermore, post-translational modifications of Swi6, such as phosphorylation, can alter the balance of interactions between the histone deacetylase Clr3 and H3K9 demethylase Epe1. The loss of Swi6 phosphorylation leads to increased Epe1 interactions and decreased heterochromatin silencing (Shimada *et al.*, 2009).

The divergent phenotypes associated with Swi6-Y and Swi6-K present an interesting case study for how minimal changes within an HP1 protein, where protein architecture is preserved, can serve as drivers of functional innovation. It is evident from our biochemistry and mass spectrometry data that these divergent effects are not due to differences in protein structure (Swi6-Y and Swi6-K form stable dimers), nucleosome binding (site-specific perturbations do not affect H3K9me binding), or interactions with Epe1. Furthermore, both variants exhibit increased chromatin occupancy *in vivo* yet produce opposite effects on epigenetic inheritance. Our findings demonstrate that simply increasing Swi6 occupancy on chromatin is insufficient to induce epigenetic inheritance. Instead, the primary deciding factor for epigenetic inheritance in *S.pombe* is the extent to which H3K9me bound Swi6 efficiently interacts with components of the rixosome complex (Holla *et al.*, 2020; Shipkovenska *et al.*, 2020).

Our results propose a new non-catalytic function for Epe1, a putative histone demethylase with no known enzymatic activity despite having structural similarities to JmjC containing histone demethylases (Trewick et al., 2005; Trewick et al., 2007). We have previously shown that point mutations, which are thought to affect Epe1 catalytic activity, lead to a loss of a direct interaction between Epe1 and Swi6 (Raiymbek *et al.*, 2020). The trade-off in protein-protein interactions that we observed in the case of Swi6-Y lends additional support to a model where Epe1 regulates epigenetic inheritance by attenuating the interaction between Swi6 and heterochromatin maintenance enhancers such as the rixosome (**Figure 6**). The molecular basis for the loss of maintenance in the case of Swi6-K needs to be clarified. We can partially rescue the maintenance defect observed in Swi6-K by additionally tethering Clr3 at the ectopic locus. These observations suggest a positive genetic interaction between Swi6-K and Clr3, leading to increased heterochromatin maintenance (**Figure 5F**). Notably, Clr3 tethering has been shown to bypass essential factors in heterochromatin inheritance, including the rescue of reduced H3K9me density, increased histone turnover, and impaired heterochromatin positioning at the

nuclear periphery (Aygun *et al.*, 2013)(Zofall, 2022). However, despite Clr3 having multifaceted rescue effects on heterochromatin, we could not restore maintenance in a *grc3* V70M background by tethering Clr3 (**Figure 5F**). Therefore, unlike many other essential maintenance regulators, the requirement for the rixosome cannot be bypassed by Clr3 during heterochromatin maintenance, which strongly suggests that the rixosome acts downstream of Clr3-mediated histone deacetylation.

Our observations support a model where the basic unit of epigenetic inheritance must involve multiprotein, Swi6-dependent complexes that assemble using H3K9me chromatin as a template (Nakayama et al., 2000). This model is consistent both with the Swi6-Y variant having increased chromatin occupancy and increased interactions with heterochromatin maintenance enhancers such as the rixosome. We envision that the stable association of Swi6 before and after DNA replication could have a crucial role in ensuring that epigenetic states remain stable and heritable across multiple generations. It is possible to envision a scenario where Swi6 binds to H3K9me heterochromatin, and the protein-protein interaction network that emerges from this binding makes its inheritance unique and distinct from euchromatin (Reinberg and Vales, 2018).

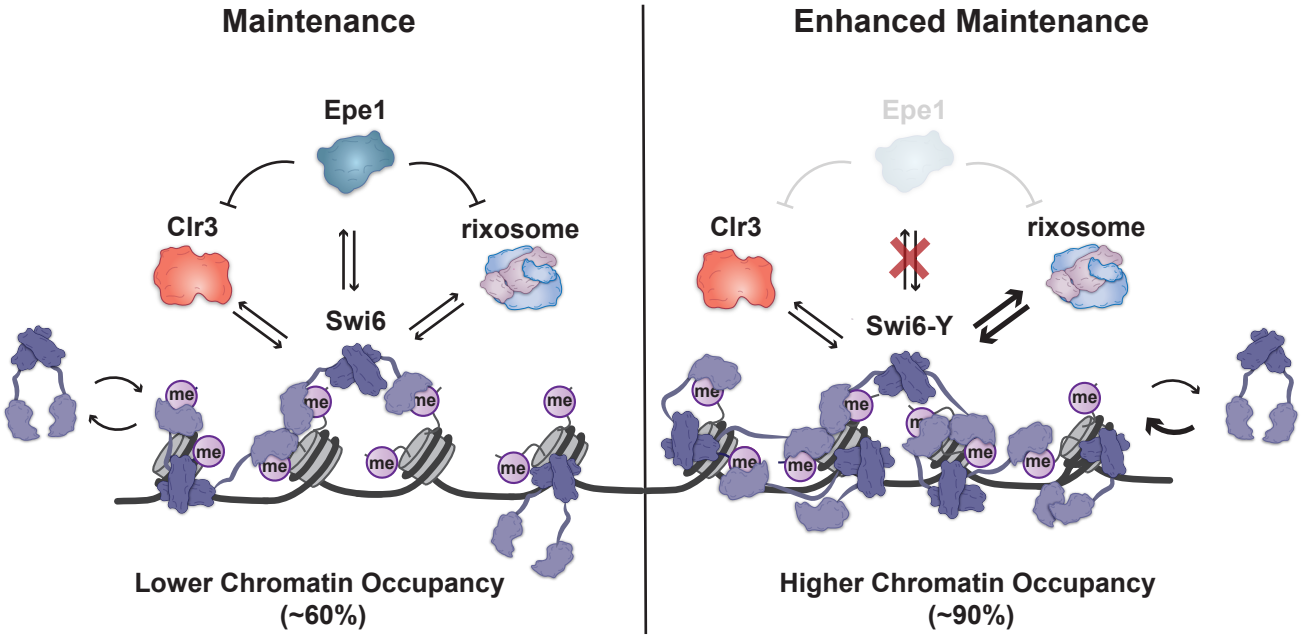

Figure 6. The Swi6-CSD dictates the inheritance capacity of heterochromatin by coordinating selective protein interactions. Model for Swi6-CSD-mediated epigenetic inheritance capacity. The CSD amino acid composition in Swi6-WT permits binding to proteins that inhibit (Epe1) and promote (Clr3 and rixosome) heterochromatin, leading to restriction of heterochromatin maintenance at the ectopic locus. Upon Swi6-Y mutation, the Epe1 interaction is lost and the rixosome interaction is upregulated, leading to enhanced heterochromatin maintenance. Swi6-Y is more chromatin-bound than Swi6-WT, indicating the chromatin landscape is altered. The rixosome is recruited to heterochromatin directly by Swi6 for heterochromatin RNA clearance. Chromatin-associated transcripts are processed for subsequent degradation, allowing for Clr4-mediated read-write heterochromatin inheritance. Therefore, our findings support a model where the regulation of Swi6-Epe1 and Swi6-rixosome interactions influence epigenetic inheritance of heterochromatin.

MATERIALS AND METHODS

Strains

All point mutation, deletion, and tagging strains were generated using published standard protocols, which include PCR-based gene targeting, the SpEDIT CRISPR/Cas9 system, or by a cross followed by random spore analysis (Bähler et al., 1998; Khare et al., 2011; Torres-Garcia et al., 2020a). All strains used in this study are listed in Supplementary Table 1.

Site-directed saturation mutagenesis library generation

The site-directed saturation mutagenesis is adapted from (Kitzman et al., 2015)). Primers were designed to contain an "NNN" degenerate sequence at every codon position within the Swi6 coding sequence and were commercially synthesized. A Swi6 plasmid template was generated using topoisomerase-based cloning. The insert sequence was generated by PCR from genomic DNA and included the Swi6 coding sequence with 500-bp flanking homology segments. The library was generated by three-step PCR. The first PCR reaction introduces the degenerate codons, the second extends the truncated PCR products from step 1, and the third adds the necessary homology for recombination at the endogenous Swi6 locus. The library was transformed into a strain where the endogenous Swi6-CSD is deleted with a ura4-kan selection marker. Positive transformants were selected by growth on FOA and loss of G418 resistance. Red or pink colonies on YE (establishment) were subsequently tested on YE+tet (maintenance). Colonies that show maintenance were considered library hits, and the Swi6 mutation was mapped using Sanger sequencing.

Expression and Purification of Recombinant Protein

Swi6 expression and purification approach was adapted based on an earlier study (Biswas *et al.*, 2022). Swi6 coding sequence was cloned into N-terminal 6XHis-tag–containing pET vectors, and mutants were generated using site-directed mutagenesis. All Swi6 proteins were purified from BL21(DE3)-RIPL *E. coli* cells. Cells were grown at 37°C to OD 0.5 to 0.8 in LB media with ampicillin (100 µg/ml), induced with 0.4 mM isopropyl-β-D-thiogalactopyranoside

(IPTG), and were grown for 16 hours at 18°C. Cells were harvested and resuspended in lysis buffer [1× phosphate-buffered saline (PBS) buffer (pH 7.3), 300 mM NaCl, 10% glycerol, 0.1% Igepal CA-630, 1 mM phenylmethylsulfonyl fluoride (PMSF), aprotonin (1 μg/ml), pepstatin A, and leupeptin] and sonicated. Cell debris was removed by centrifugation at 25,000*g* for 35 min. Cell lysates were incubated with HisPur NiNTA resin (Thermo Fisher Scientific) at 4°C for at least 2 hours. The resin was washed with lysis buffer, and protein was eluted [20 mM Hepes (pH 7.5), 100 mM KCl, 10% glycerol, and 500 mM imidazole] and incubated with the corresponding protease (Ulp1 or TEV) overnight at 4°C. After cleavage of 6XHis-tag, the products were further isolated by anion exchange chromatography using a HiTRAP Q HP column (Cytiva) and size exclusion chromatography using a Superdex200 10/300 (Cytiva) column. Proteins were dialyzed into storage buffer [20 mM Hepes, 100 mM KCl, 10% glycerol, and 1 mM dithiothreitol (DTT)]. Protein concentrations were determined using ultraviolet (UV) absorption measurements at 280 nm and molecular weights (MWs) and extinction coefficients computationally determined for Swi6-WT (MW = 37,292.6 g/mol, ε = 41,035 M^{-1} cm^{-1}), Swi6-L315E (MW = 37,308.6 g/mol, ε = 41,035 M^{-1} cm^{-1}), Swi6-T278Y (MW = 37,354.7 g/mol, ε = 42,525 M^{-1} cm^{-1}), and Swi6-T278K (MW = 37,319.7 g/mol, ε = 41,035 M^{-1} cm^{-1}) using the Expasy ProtParam tool. Protein was further equalized using SDS-PAGE densitometry quantification. Epe1 was purified as described previously (Raiymbek *et al.*, 2020). MBP-His-TEV-Epe1 was cloned into a pFastBac vector (Thermo Fisher Scientific) and used for Bacmid generation. Low-titer baculoviruses were produced by transfecting Bacmid into Sf21 cells using Cellfectin II reagent (Gibco). Full-length *S.pombe* Epe1 protein (wild-type and mutant) was expressed in Hi5 cells infected by high titer baculovirus, amplified from Sf21 cells. After 44 h of infection, Hi5 cells were harvested and lysed in buffer A (30 mM Tris-HCl (pH 8.0), 500 mM NaCl, 5 mM EDTA, 5 mM β-mercaptoethanol with protease inhibitor cocktails) using Emulsiflex-C3 (Avestin). The cleared cell lysate was applied to Amylose resin (New England Biolabs), followed by washing with buffer A and elution with buffer A containing 10 mM maltose. Proteins

were further purified using a Superdex 200 (GE Healthcare) size exclusion column. The protein was concentrated in a storage buffer containing 30 mM Tris-HCl (pH 8.0), 500 mM NaCl, 30% glycerol, and 1 mM TCEP.

Total protein extraction from *S.pombe*

To detect protein expression in strains containing Swi6 mutants and tagged proteins, protein extracts were prepared using Trichloroacetic Acid (TCA) precipitation. Strains were grown in liquid yeast extract supplemented with adenine (YEA) for 16 hours at 32°C, and 7 ODs worth of cells were harvested. Cell pellets were washed with 1 mL of ice-cold water and resuspended in 150 µL of YEX Buffer (1.85 M NaOH, 7.5% beta-mercaptoethanol). After 10 minutes of incubation on ice, protein precipitation was performed by adding 150 µL of 50% TCA (~3 N) and mixing by inversion. The extracts were then incubated for 10 minutes on ice, pelleted by centrifugation, and excess TCA was carefully removed. The protein extracts were resuspended in 2X SDS sample buffer (125 mM Tris-Base pH 6.8, 8M urea, 5% SDS, 20% glycerol, 5% BME) and centrifuged for 5 minutes to clear cell debris. Samples were analyzed by western blotting, as described below.

Western Blotting

Protein samples were resolved by gel electrophoresis on 4–20% Mini-PROTEAN® TGX Stain-Free™ Protein Gels. Immunoblotting was performed using the BioRad Trans-Blot Turbo Transfer System, and transfer was performed at 2.5A and 25V for 7 minutes onto 0.2 µm Nitrocellulose. Membranes were blocked using 5% non-fat dry milk in Tris-buffered saline pH 7.5 with 0.1% Tween-20 (TBST) for 1 hour. The membrane was then incubated with the primary antibody at an optimized concentration overnight at 4°C. Following incubation, the membrane was washed 3 times with TBST and incubated with the appropriate secondary antibody for 1 hour at room temperature. After the incubation, the membrane was washed 3 times with TBST and incubated with SuperSignal West Pico/Femto PLUS Chemiluminescent Substrate. The membrane was imaged for chemiluminescence on a Bio-Rad ChemiDoc.

Coimmunoprecipitation measurements to detect Epe1-Swi6 interaction (CoIP)

CoIP experiments were performed as described previously (Raiymbek *et al.*, 2020). 1.5 L of fission yeast cells were grown in YEA medium at 32°C to an OD_{600} = 3.5 and harvested by centrifugation. The cell pellets were washed with 10 ml TBS pH 7.5, resuspended in 1.5 ml lysis buffer (30 mM HEPES pH 7.5, 100 mM NaCl, 0.25% Triton X-100, 5 mM $MgCl_2$,1 mM DTT), and the cell suspension was snap-frozen into liquid nitrogen drop-wise and cryogenically ground using a SPEX 6875D Freezer Mill. The frozen cell powder was stored at -80˚C, thawed at room temperature, and resuspended in an additional 10 ml of lysis buffer with a protease inhibitor cocktail and 1 mM PMSF. Cell lysates were subjected to two rounds of centrifugation at 18000 rpm for 5 and 30 mins in a JA-25.50 rotor (Beckman). Protein levels were normalized for coimmunoprecipitation and immunoblot analysis using a Bradford Assay. Protein G Magnetic Beads were pre-incubated with V5 antibody (A01724, Genscript) for 4 h and crosslinked with 10 volumes of crosslinking buffer containing 20 mM DMP (3 mg DMP/ml of 0.2 M Boric Acid pH 9) for 30 min at room temperature by rotating. Crosslinking was quenched by washing twice and incubated with 0.2 M ethanolamine pH 8 for 2 h at room temperature. The cell lysates were then incubated with antibody crosslinked beads for 3 h at 4°C. Beads were washed thrice in 1 ml lysis buffer for 5 mins each, then eluted with 500 µl of 10 mM ammonium hydroxide. The ammonium hydroxide was evaporated using a speed vac (SPC-100H) for 5 h and resuspended in SDS sample buffer. Samples were resolved using SDS–polyacrylamide gel electrophoresis (SDS-PAGE) and transferred to PVDF membranes. Immunoblotting was performed by blocking the PVDF membrane in Tris-buffered saline (TBS) pH 7.5 with 0.1% Tween-20 (TBST) containing 5% non-fat dry milk and subsequently probed with desired primary antibodies and secondary antibodies. Blots were developed by enhanced chemiluminescence (ECL) method and detected using a Bio-Rad ChemiDoc Imaging System.

In vitro binding assay to detect Epe1-Swi6 interaction

In vitro binding assays were performed by immobilizing recombinant 3X FLAG-Swi6 on 25 µl of FLAG M2 beads, which were incubated with three different concentrations of recombinant MBP-Epe1 fusion proteins in 600 µl binding buffer containing 20 mM HEPES pH 7.5, 150 mM NaCl, 5 mM $MgCl_2$, 10% glycerol, 0.25% Triton -X 100, 1 mM DTT. Reactions were incubated at 4°C for 2 h and washed three times in 1 ml washing buffer (20 mM HEPES pH 7.5, 150 mM NaCl, 5 mM $MgCl_2$, 10% glycerol, 0.25% Triton -X 100, 1 mM DTT) for 5 min each, then 30µl of SDS sample buffer was added followed by incubation at 95°C for 5 min. Proteins were separated through SDS-PAGE and transferred to a PVDF membrane followed by incubation with anti-MBP monoclonal antibody (E8032S, NEB) and M2 Flag antibody (A8592, Sigma). Western blot data for _in vitro_ binding assays were analyzed using ImageJ software. The exposure times for the interaction assays were chosen and differed in each experiment to capture differences in the interaction between Epe1 and Swi6 depending on the assay conditions. Assays performed on different blots cannot be compared, but samples loaded on the same blot can be readily compared.

Tandem-mass tag affinity purification mass spec

Protein levels were normalized between the triplicate samples by silver stain. Dried eluates were sent to the Thermo Fisher Center for Multiplexed Proteomics at Harvard Medical School for further processing and analysis. Dried samples were resuspended in 20 mM EPPS, pH 8.5. Samples were reduced with TCEP, alkylated with iodoacetamide, and further reduced with DTT. Proteins were extracted with SP3 beads. Samples were digested overnight at room temperature with Lys-C, followed by digestion with trypsin for 6 hours at 37˚C. Protein samples were labeled with TMTPro reagants, and complete labeling was confirmed. All samples were pooled and desalted by stage-tip. Peptides were analyzed on an Orbitrap Eclipse Mass Spectrometer. MS2 spectra were searched using the COMET algorithm against an _S.pombe_ Uniprot composite database (downloaded in 2023) containing its reversed complement and

known contaminants. For proteome, Peptide spectral matches were filtered to a 1% false discovery rate (FDR) using the target-decoy strategy combined with linear discriminant analysis. The proteins were filtered to a <1% FDR and quantified only from peptides with a summed SN threshold of >120.

Silencing Assays

Cells were grown in 3 ml of yeast extract containing adenine (YEA) at 32°C overnight. Cells were washed twice in water and then resuspended to a concentration of `~10^7 cells/ml. Ten-fold serial dilutions (~5μL) were plated on YE plates to evaluate establishment and YE+AHT to evaluate maintenance. Plates were incubated for 2-3 days before the results were cataloged.

Chromatin immunoprecipitation (ChIP)

30 ml of cells were grown to late log phase (OD_{600}-1.8-2.2) in yeast extract supplemented with adenine (YEA) or YEA containing tetracycline (2.5 μg/ml) and fixed with 1% formaldehyde for 15 min at room temperature (RT). 130 mM glycine was added to quench the reaction and incubated for 5 min at RT. The cells were harvested by centrifugation and washed with TBS (50 mM Tris, pH 7.6, 500 mM NaCl). Cell pellets were resuspended in 300 μL lysis buffer (50 mM HEPES-KOH, pH 7.5, 100 mM NaCl, 1mM EDTA, 1% Triton X-100, 0.1% SDS, and protease inhibitors) to which 500 μL 0.5 mm glass beads were added. Cell lysis was carried out by bead beating using Omni Bead Ruptor at 3000 rpm x 30sec x 10 cycles. Tubes were punctured, and the flow-through was collected in a new tube by centrifugation, which was subjected to sonication to obtain fragment sizes of roughly 100-500 bp long. After sonication, the extract was centrifuged for 15 min at 13000 rpm at 4°C. The soluble chromatin was transferred to a fresh tube and normalized for protein concentration by Bradford assay. For each normalized sample, 25 μL lysate was saved as input, to which 225 μL of 1xTE/1% SDS were added (TE: 50 mM Tris pH 8.0, 1 mM EDTA). Protein A Dynabeads were preincubated with H3K9me2 antibody (Abcam, ab1220) or H3K9me3 antibody (39161, Active Motif). For each

728 immunoprecipitation, we used 2 µg H3K9me2 antibody (Abcam, ab1220) and 2 µg H3K9me3
729 antibody (39161, Active Motif). Samples were incubated for 3h at 4°C. The beads were
730 collected on magnetic stands and washed 3 times with 1 mL lysis buffer and once with 1 mL TE.
731 For eluting bound chromatin, 100 µL elution buffer I (50 mM Tris pH 8.0, 10 mM EDTA, 1%
732 SDS) was added, and the samples were incubated at 65°C for 5 min. The eluate was collected
733 and incubated with 150 µL 1xTE/0.67% SDS in the same way. Input and immunoprecipitated
734 samples were incubated overnight at 65°C to reverse crosslink. 60 µg glycogen, 100 µg
735 proteinase K (Roche), 44 µL of 5M LiCl, and 250 µL of 1xTE were added to each sample, and
736 incubation was continued at 55°C for 1h. Phenol/chloroform extraction was carried out for all the
737 samples, followed by ethanol precipitation. Immuno-precipitated DNA was resuspended in 100
738 µL of 10 mM Tris pH 7.5 and 50 mM NaCl. ChIP experiments were analyzed using quantitative
739 PCR with Taq polymerase and SYBR Green using a CFX Opus 384 Real-Time PCR System.
740 PCR primers are listed in Supplementary Table 2.

741 **ChIP-Seq library preparation and processing**

742 ChIP-seq libraries were prepared and processed as described previously (Seman *et al.*,
743 2023). Libraries were constructed using the manufacturer's guidelines in the NEBNext® Ultra™
744 II FS DNA Library Prep Kit for Illumina, using 1ng of starting material. Barcoded libraries were
745 pooled and sequenced with next-generation sequencing. First, raw reads were demultiplexed by
746 barcode. Then, the sequences were trimmed with Trimmomatic, aligned with BWA, and
747 normalized by reads per million (Bolger et al., 2014; Li and Durbin, 2010). The reads were
748 visualized with IGV. For further analysis, peaks were called using MACS2 with -g 12.57x 10^{-6} in
749 broad mode with a cutoff of 0.05 (Zhang et al., 2008b). Heatmaps were generated using
750 deepTools v3.5.1 (Ramírez et al., 2016).

751 **RNA extraction**

752 10 mL of cells were grown to late log phase (OD_{600}-1.8-2.2) in yeast extract
753 supplemented with adenine. Cells were resuspended in 750 µL TES buffer (0.01 M Tris pH7.5,

754 0.01 M EDTA, 0.5% SDS). Immediately, 750 µL of acidic phenol-chloroform was added and
755 vortexed for 2 minutes. Samples were incubated at 65°C for 40 minutes while vortexing for 20
756 seconds every ten minutes. The aqueous phase was separated by centrifuging in Phase Lock
757 tubes for 5 minutes at 13000 rpm at 4°C. The aqueous phase was transferred to new tubes, and
758 ethanol precipitated. After extraction, RNA was treated with DNase. Then, the RNA was cleaned
759 using RNeasy Mini kits (Qiagen). cDNA was prepared using oligodT and SuperScript III
760 Reverse Transcriptase (Invitrogen). The cDNA was then used for qPCR with SYBR Green and
761 Taq polymerase on a CFX OPUS 384 Real-Time PCR System. RNA levels were quantified
762 using ΔC_T compared to tubulin *(tub1*) RNA levels. PCR primers are listed in Supplementary
763 Table 2.

764 **Mass Photometry**

765 All mass photometry experiments were performed using full-length recombinant Swi6
766 protein at the Center for Macromolecular Interactions at Harvard Medical School using a Refeyn
767 TwoMP instrument. Before taking measurements, the instrument was calibrated using a protein
768 standard containing 10 nM β-amylase (Sigma Aldrich A8781) and 3 nM Thyroglobulin (Sigma-
769 Aldrich 609310). Swi6 proteins were diluted to 100 nM in 20 mM HEPES pH 7.5, 100 mM KCl
770 immediately before taking measurements. For each measurement, the objective was focused
771 using 20 mM HEPES pH 7.5, 100 mM KCl, and the corresponding volume of 100 nM Swi6 was
772 added to the droplet to achieve the desired final concentration (2.5-20 nM). Sample data was
773 collected immediately. Figures and Gaussian fits of the resulting data were generated using the
774 Refeyn DiscoverMP software. Apparent dimerization constants (K_{dim}) were determined by
775 relative molecular abundance of the monomer and dimer populations at known Swi6
776 concentrations (Fineberg et al., 2020; Soltermann *et al.*, 2020).

777 **AlphaFold2-multimer (AF-M) structural prediction**

AlphaFold2 Multimer was used to predict protein-protein interactions using the Cosmic[2] Science Gateway server (Cianfrocco et al., 2017; Evans *et al.*, 2022). In all cases, we obtained 5 models with 3 recycles, and all structures were unrelaxed. Protein structures were plotted using Chimera (Pettersen et al., 2004). We further analyzed our structures using a published pipeline to determine interface statistics from predicted multimer structural models (Lim et al., 2023). This pipeline identifies all interchain interactions within 8 angstroms across all five models. The pipeline also provides several metrics to score the confidence of the predicted multimer interfaces accounting for the consistency of interactions and pLDDT scores across all models (**Supplemental Figures 4F, 5F, 6F, 10F**).

***S.pombe* live-cell imaging**

Yeast strains containing a copy of PAmCherry-Swi6 or a PAmCherry-Swi6 mutant under the control of the native Swi6 promoter were grown in standard complete YES media (US Biological, catalog no. Y2060) containing the full complement of yeast amino acids and incubated overnight at 32°C. This initial culture was diluted and incubated at 25°C with shaking to reach an optical density at 600 nm (OD_{600}) of ~0.5. To maintain cells in an exponential phase and eliminate extranuclear vacuole formation, the culture was maintained at OD_{600} ~0.5 for 2 days, diluting at ~12-hour intervals. To prepare agarose pads for imaging, cells were pipetted onto a pad of 2% agarose prepared in YES media with 0.1 mM *N*-propyl gallate (Sigma-Aldrich, catalog no. P-3130) and 1% gelatin (Millipore, catalog no. 04055) as additives to reduce phototoxicity during imaging. *S.pombe* cells were imaged at room temperature with a 100x 1.40 numerical aperture (NA) oil-immersion objective in an Olympus IX-71 inverted microscope. First, the fluorescent background was decreased by exposure to 488 nm light (Coherent Sapphire, 200 W/cm^2 for 20 to 40 s). A 406-nm laser (Coherent Cube, 405-100; 102 W/cm^2) was used for photoactivation (200-ms activation time), and a 561-nm laser (Coherent Sapphire, 561-50; 163 W/cm^2) was used for imaging. Images were acquired at 40-ms exposure time per frame. The fluorescence emission was filtered with a Semrock LL02-561-12.5 long-pass filter and a Chroma

ZT488/561rpc 488/561 dichroic mirror to eliminate the 561 nm excitation source and imaged using a 512 × 512-pixel Photometrics Evolve EMCCD camera.

Single-molecule trajectory analysis

Recorded Swi6-PAmCherry single-molecule positions were detected and localized with two-dimensional Gaussian fitting with home-built MATLAB software as previously described and connected into trajectories using the Hungarian algorithm (Isaacoff et al., 2019; Munkres, 1957; Rowland and Biteen, 2017). These single-molecule trajectory datasets were analyzed by a nonparametric Bayesian framework to reveal heterogeneous dynamics (Karslake *et al.*, 2021). This SMAUG algorithm uses nonparametric Bayesian statistics and Gibbs sampling to identify the number of distinct mobility states in the single molecule tracking dataset in an iterative manner. It also infers parameters, including weight fraction and average apparent diffusion coefficient for each mobility state, assuming a Brownian motion model. To ensure that even rare events were captured, we collected more than 10,000 steps in our single-molecule tracking dataset for each measured strain, and we ran the algorithm over >10,000 iterations to achieve a thoroughly mixed state space. The state number and associated parameters were updated in each iteration of the SMAUG algorithm and saved after convergence. The final estimation shows the data after convergence for iterations with the most frequent state number. Each mobility state is assigned a distinct color, and for each saved iteration, the average diffusion coefficient of that state is plotted against the weight fraction. The distributions of estimates over the iterations give the uncertainty in the determination of the parameters. For measurement of static molecules in fixed *S.pombe* cells, SMAUG converges to a single state with D_{avg} = 0.0041 ± 0.0003 μm^2/s. The average localization error for single-molecule localizations in this fixed-cell imaging is 32.6 nm. To benchmark against a model that overcomes potential overfitting of the Bayesian model, we also applied the DPSP package to acquire the posterior occupancy distribution for diffusion coefficients of Swi6 and variants (Heckert *et al.*, 2022). The DPSP package uses a Dirichlet process mixture model to acquire the posterior probability distribution

for each dataset. The same trajectory datasets used in SMAUG analysis were stored in csv format and analyzed with the Python package DPSP under default parameter settings and corresponding pixel size and frame interval (https://github.com/alecheckert/dpsp).

Nucleosome Electrophoretic Mobility Shift Assays (EMSAs)

Samples were prepared by varying concentrations of Swi6 while keeping substrate concentration, i.e. 10 nM mononucleosomes (H3K9me0 and H3K9me3, Epicypher catalog nos. 16-0006 and 16-0315-20) constant in binding buffer [20 mM Hepes (pH 7.5), 4 mM tris, 80 mM KCl, 0.1% Igepal CA-630, 0.2 mM EDTA, 2 mM DTT, and 10% glycerol]. Samples were incubated at 30°C for 45 min. A 0.5x tris-borate EDTA 6% acrylamide:bis-acrylamide 37.5:1 gel was pre-run at RT for at least 1 hour at 75 V. Reactions were loaded on the gel and ran under the same conditions for 3 hours. Gels were poststained for 2 hours with polyacrylamide gel electrophoresis (PAGE) GelRed DNA stain (Biotium) and imaged using a Typhoon Imager. The unbound nucleosome band was quantified using ImageJ, and binding curves were fit using nonlinear regression (Prism 9).

DATA AVAILABILITY

Sequencing data has been deposited in GEO under accession code GSE248428.

ACKNOWLEDGMENTS

The authors declare no competing interests. We thank Danesh Moazed for sharing the fission yeast strains used in this study. We thank Saarang Gopinath for his support in obtaining preliminary data during the initial phase of this study. This work was supported by the National Science Foundation (grant no. EF-2316281 to K.R. and J.S.B), National Institutes of Health (grant nos. R35GM137832 to K.R.; T32GM007544 to A.A and A.L.; and T32GM007315 to M.S) and American Cancer Society (grant no. RSG-22-117-01-DMC to K.R.) Molecular graphics and analyses were performed with UCSF Chimera, developed by the Resource for Biocomputing, Visualization, and Informatics at the University of California, San Francisco, with support from NIH P41-GM103311. AlphaFold-Multimer-based *in silico* models were generated using Cosmic2

856 (Cianfrocco *et al.*, 2017). We thank the Center for Macromolecular Interactions at Harvard

857 Medical School and the Thermo Fisher Scientific Center for Multiplex Proteomics at Harvard

858 Medical School for their support.

859 **REFERENCES**

Allfrey, V.G., Faulkner, R., and Mirsky, A.E. (1964). Acetylation and methylation of histones and their possible role in the regulation of RNA synthesis. Proc Natl Acad Sci U S A *51*, 786-794. 10.1073/pnas.51.5.786.

Allshire, R.C., and Ekwall, K. (2015). Epigenetic Regulation of Chromatin States in Schizosaccharomyces pombe. Cold Spring Harb Perspect Biol *7*, a018770. 10.1101/cshperspect.a018770.

Allshire, R.C., Javerzat, J.P., Redhead, N.J., and Cranston, G. (1994). Position effect variegation at fission yeast centromeres. Cell *76*, 157-169. 10.1016/0092-8674(94)90180-5.

Asor, R., and Kukura, P. (2022). Characterising biomolecular interactions and dynamics with mass photometry. Current Opinion in Chemical Biology *68*, 102132. https://doi.org/10.1016/j.cbpa.2022.102132.

Audergon, P.N.C.B., Catania, S., Kagansky, A., Tong, P., Shukla, M., Pidoux, A.L., and Allshire, R.C. (2015). Restricted epigenetic inheritance of H3K9 methylation. Science *348*, 132-135. doi:10.1126/science.1260638.

Aygun, O., Mehta, S., and Grewal, S.I. (2013). HDAC-mediated suppression of histone turnover promotes epigenetic stability of heterochromatin. Nat Struct Mol Biol *20*, 547-554. 10.1038/nsmb.2565.

Bähler, J., Wu, J.Q., Longtine, M.S., Shah, N.G., McKenzie, A., 3rd, Steever, A.B., Wach, A., Philippsen, P., and Pringle, J.R. (1998). Heterologous modules for efficient and versatile PCR-based gene targeting in Schizosaccharomyces pombe. Yeast *14*, 943-951. 10.1002/(sici)1097-0061(199807)14:10<943::Aid-yea292>3.0.Co;2-y.

Bannister, A.J., Zegerman, P., Partridge, J.F., Miska, E.A., Thomas, J.O., Allshire, R.C., and Kouzarides, T. (2001). Selective recognition of methylated lysine 9 on histone H3 by the HP1 chromo domain. Nature *410*, 120-124. 10.1038/35065138.

Bao, K., Shan, C.-M., Chen, X., Raiymbek, G., Monroe, J.G., Fang, Y., Toda, T., Koutmou, K.S., Ragunathan, K., Lu, C., et al. (2022). The cAMP signaling pathway regulates Epe1 protein levels and heterochromatin assembly. PLOS Genetics *18*, e1010049. 10.1371/journal.pgen.1010049.

Bao, K., Shan, C.M., Moresco, J., Yates, J., 3rd, and Jia, S. (2019). Anti-silencing factor Epe1 associates with SAGA to regulate transcription within heterochromatin. Genes Dev *33*, 116-126. 10.1101/gad.318030.118.

Baumgartner, L., Handler, D., Platzer, S.W., Yu, C., Duchek, P., and Brennecke, J. (2022). The Drosophila ZAD zinc finger protein Kipferl guides Rhino to piRNA clusters. eLife *11*. 10.7554/eLife.80067.

Baumgartner, L., Ipsaro, J.J., Hohmann, U., Handler, D., Schleiffer, A., Duchek, P., and Brennecke, J. (2023). Evolutionary adaptation of the chromodomain of the HP1-protein Rhino allows the integration of chromatin and DNA sequence signals. bioRxiv, 2023.2009.2029.560096. 10.1101/2023.09.29.560096.

Biswas, S., Chen, Z., Karslake, J.D., Farhat, A., Ames, A., Raiymbek, G., Freddolino, P.L., Biteen, J.S., and Ragunathan, K. (2022). HP1 oligomerization compensates for low-affinity H3K9me recognition and provides a tunable mechanism for heterochromatin-specific localization. Science Advances *8*, eabk0793. doi:10.1126/sciadv.abk0793.

Bolger, A.M., Lohse, M., and Usadel, B. (2014). Trimmomatic: a flexible trimmer for Illumina sequence data. Bioinformatics *30*, 2114-2120. 10.1093/bioinformatics/btu170.

Brasher, S.V., Smith, B.O., Fogh, R.H., Nietlispach, D., Thiru, A., Nielsen, P.R., Broadhurst, R.W., Ball, L.J., Murzina, N.V., and Laue, E.D. (2000). The structure of mouse HP1 suggests a unique mode of single peptide recognition by the shadow chromo domain dimer. The EMBO Journal *19*, 1587-1597. https://doi.org/10.1093/emboj/19.7.1587.

Braun, S., Garcia, J.F., Rowley, M., Rougemaille, M., Shankar, S., and Madhani, H.D. (2011). The Cul4-Ddb1(Cdt)² ubiquitin ligase inhibits invasion of a boundary-associated antisilencing factor into heterochromatin. Cell *144*, 41-54. 10.1016/j.cell.2010.11.051.

Brickner, J.H. (2023). Inheritance of epigenetic transcriptional memory through read–write replication of a histone modification. Annals of the New York Academy of Sciences *1526*, 50-58. https://doi.org/10.1111/nyas.15033.

Canzio, D., Chang, E.Y., Shankar, S., Kuchenbecker, K.M., Simon, M.D., Madhani, H.D., Narlikar, G.J., and Al-Sady, B. (2011). Chromodomain-mediated oligomerization of HP1 suggests a nucleosome-bridging mechanism for heterochromatin assembly. Mol Cell *41*, 67-81. 10.1016/j.molcel.2010.12.016.

Canzio, D., Larson, A., and Narlikar, G.J. (2014). Mechanisms of functional promiscuity by HP1 proteins. Trends in Cell Biology *24*, 377-386. https://doi.org/10.1016/j.tcb.2014.01.002.

Canzio, D., Liao, M., Naber, N., Pate, E., Larson, A., Wu, S., Marina, D.B., Garcia, J.F., Madhani, H.D., Cooke, R., et al. (2013). A conformational switch in HP1 releases auto-inhibition to drive heterochromatin assembly. Nature *496*, 377-381. 10.1038/nature12032.

Cianfrocco, M.A., Wong-Barnum, M., Youn, C., Wagner, R., and Leschziner, A. (2017). Cosmic2. Proceedings of the Practice and Experience in Advanced Research Computing 2017 on Sustainability, Success and Impact.

Cowieson, N.P., Partridge, J.F., Allshire, R.C., and McLaughlin, P.J. (2000). Dimerisation of a chromo shadow domain and distinctions from the chromodomain as revealed by structural analysis. Current Biology *10*, 517-525. https://doi.org/10.1016/S0960-9822(00)00467-X.

Eeftens, J.M., Kapoor, M., Michieletto, D., and Brangwynne, C.P. (2021). Polycomb condensates can promote epigenetic marks but are not required for sustained chromatin compaction. Nature Communications *12*. 10.1038/s41467-021-26147-5.

Evans, R., O'Neill, M., Pritzel, A., Antropova, N., Senior, A., Green, T., Žídek, A., Bates, R., Blackwell, S., Yim, J., et al. (2022). Protein complex prediction with AlphaFold-Multimer. bioRxiv. 10.1101/2021.10.04.463034.

Fineberg, A., Surrey, T., and Kukura, P. (2020). Quantifying the Monomer-Dimer Equilibrium of Tubulin with Mass Photometry. J Mol Biol *432*, 6168-6172. 10.1016/j.jmb.2020.10.013.

Fischer, T., Cui, B., Dhakshnamoorthy, J., Zhou, M., Rubin, C., Zofall, M., Veenstra, T.D., and Grewal, S.I.S. (2009). Diverse roles of HP1 proteins in heterochromatin assembly and functions in fission yeast. Proceedings of the National Academy of Sciences *106*, 8998-9003. 10.1073/pnas.0813063106.

Flavahan, W.A., Gaskell, E., and Bernstein, B.E. (2017). Epigenetic plasticity and the hallmarks of cancer. Science *357*. 10.1126/science.aal2380.

Franklin, K.A., Shields, C.E., and Haynes, K.A. (2022). Beyond the marks: reader-effectors as drivers of epigenetics and chromatin engineering. Trends Biochem Sci *47*, 417-432. 10.1016/j.tibs.2022.03.002.

Haldar, S., Saini, A., Nanda, J.S., Saini, S., and Singh, J. (2011). Role of Swi6/HP1 self-association-mediated recruitment of Clr4/Suv39 in establishment and maintenance of heterochromatin in fission yeast. J Biol Chem *286*, 9308-9320. 10.1074/jbc.M110.143198.

Hanahan, D., and Weinberg, Robert A. (2011). Hallmarks of Cancer: The Next Generation. Cell *144*, 646-674. 10.1016/j.cell.2011.02.013.

Hayashi, A., Ishida, M., Kawaguchi, R., Urano, T., Murakami, Y., and Nakayama, J.-i. (2012). Heterochromatin protein 1 homologue Swi6 acts in concert with Ers1 to regulate RNAi-directed heterochromatin assembly. Proceedings of the National Academy of Sciences *109*, 6159-6164. 10.1073/pnas.1116972109.

Heckert, A., Dahal, L., Tjian, R., and Darzacq, X. (2022). Recovering mixtures of fast-diffusing states from short single-particle trajectories. eLife *11*, e70169. 10.7554/eLife.70169.

Helleu, Q., and Levine, M.T. (2018). Recurrent Amplification of the Heterochromatin Protein 1 (HP1) Gene Family across Diptera. Mol Biol Evol *35*, 2375-2389. 10.1093/molbev/msy128.

Hildebrand, E.M., and Dekker, J. (2020). Mechanisms and Functions of Chromosome Compartmentalization. Trends in Biochemical Sciences *45*, 385-396. 10.1016/j.tibs.2020.01.002.

Hiragami-Hamada, K., Shinmyozu, K., Hamada, D., Tatsu, Y., Uegaki, K., Fujiwara, S., and Nakayama, J. (2011). N-terminal phosphorylation of HP1{alpha} promotes its chromatin binding. Mol Cell Biol *31*, 1186-1200. 10.1128/mcb.01012-10.

Hirano, Y., Asakawa, H., Sakuno, T., Haraguchi, T., and Hiraoka, Y. (2020). Nuclear Envelope Proteins Modulating the Heterochromatin Formation and Functions in Fission Yeast. Cells *9*, 1908.

Holla, S., Dhakshnamoorthy, J., Folco, H.D., Balachandran, V., Xiao, H., Sun, L.-l., Wheeler, D., Zofall, M., and Grewal, S.I.S. (2020). Positioning Heterochromatin at the Nuclear Periphery Suppresses Histone Turnover to Promote Epigenetic Inheritance. Cell *180*, 150-164.e115. https://doi.org/10.1016/j.cell.2019.12.004.

Iglesias, N., Paulo, J.A., Tatarakis, A., Wang, X., Edwards, A.L., Bhanu, N.V., Garcia, B.A., Haas, W., Gygi, S.P., and Moazed, D. (2020). Native Chromatin Proteomics Reveals a Role for Specific Nucleoporins in Heterochromatin Organization and Maintenance. Molecular Cell *77*, 51-66.e58. 10.1016/j.molcel.2019.10.018.

Isaac, R.S., Sanulli, S., Tibble, R., Hornsby, M., Ravalin, M., Craik, C.S., Gross, J.D., and Narlikar, G.J. (2017). Biochemical Basis for Distinct Roles of the Heterochromatin Proteins Swi6 and Chp2. J Mol Biol *429*, 3666-3677. 10.1016/j.jmb.2017.09.012.

Isaacoff, B.P., Li, Y., Lee, S.A., and Biteen, J.S. (2019). SMALL-LABS: Measuring Single-Molecule Intensity and Position in Obscuring Backgrounds. Biophysical Journal *116*, 975-982. https://doi.org/10.1016/j.bpj.2019.02.006.

Ivanova, A.V., Bonaduce, M.J., Ivanov, S.V., and Klar, A.J.S. (1998). The chromo and SET domains of the Clr4 protein are essential for silencing in fission yeast. Nature Genetics *19*, 192-195. 10.1038/566.

Jacobs, S.A., and Khorasanizadeh, S. (2002). Structure of HP1 chromodomain bound to a lysine 9-methylated histone H3 tail. Science *295*, 2080-2083. 10.1126/science.1069473.

Jacobs, S.A., Taverna, S.D., Zhang, Y., Briggs, S.D., Li, J., Eissenberg, J.C., Allis, C.D., and Khorasanizadeh, S. (2001). Specificity of the HP1 chromo domain for the methylated N-terminus of histone H3. Embo j *20*, 5232-5241. 10.1093/emboj/20.18.5232.

James, T.C., and Elgin, S.C.R. (2023). Identification of a Nonhistone Chromosomal Protein Associated with Heterochromatin in Drosophila melanogaster and Its Gene. Molecular and Cellular Biology *6*, 3862-3872. 10.1128/mcb.6.11.3862-3872.1986.

Kang, J., Chaudhary, J., Dong, H., Kim, S., Brautigam, C.A., and Yu, H. (2011). Mitotic centromeric targeting of HP1 and its binding to Sgo1 are dispensable for sister-chromatid cohesion in human cells. Mol Biol Cell *22*, 1181-1190. 10.1091/mbc.E11-01-0009.

Karslake, J.D., Donarski, E.D., Shelby, S.A., Demey, L.M., DiRita, V.J., Veatch, S.L., and Biteen, J.S. (2021). SMAUG: Analyzing single-molecule tracks with nonparametric Bayesian statistics. Methods *193*, 16-26. 10.1016/j.ymeth.2020.03.008.

Khare, A.K., Singh, B., and Singh, J. (2011). A fast and inexpensive method for random spore analysis in Schizosaccharomyces pombe. Yeast *28*, 527-533. https://doi.org/10.1002/yea.1855.

Kitzman, J.O., Starita, L.M., Lo, R.S., Fields, S., and Shendure, J. (2015). Massively parallel single-amino-acid mutagenesis. Nat Methods *12*, 203-206, 204 p following 206. 10.1038/nmeth.3223.

Larson, A.G., Elnatan, D., Keenen, M.M., Trnka, M.J., Johnston, J.B., Burlingame, A.L., Agard, D.A., Redding, S., and Narlikar, G.J. (2017). Liquid droplet formation by HP1α suggests a role for phase separation in heterochromatin. Nature *547*, 236-240. 10.1038/nature22822.

Larson, A.G., and Narlikar, G.J. (2018). The Role of Phase Separation in Heterochromatin Formation, Function, and Regulation. Biochemistry *57*, 2540-2548. 10.1021/acs.biochem.8b00401.

Leopold, K., Stirpe, A., and Schalch, T. (2019). Transcriptional gene silencing requires dedicated interaction between HP1 protein Chp2 and chromatin remodeler Mit1. Genes & Development *33*, 565-577. 10.1101/gad.320440.118.
Levine, M.T., McCoy, C., Vermaak, D., Lee, Y.C.G., Hiatt, M.A., Matsen, F.A., and Malik, H.S. (2012). Phylogenomic Analysis Reveals Dynamic Evolutionary History of the Drosophila Heterochromatin Protein 1 (HP1) Gene Family. PLOS Genetics *8*, e1002729. 10.1371/journal.pgen.1002729.
Li, H., and Durbin, R. (2010). Fast and accurate long-read alignment with Burrows–Wheeler transform. Bioinformatics *26*, 589-595. 10.1093/bioinformatics/btp698.
Lim, Y., Tamayo-Orrego, L., Schmid, E., Tarnauskaite, Z., Kochenova, O.V., Gruar, R., Muramatsu, S., Lynch, L., Schlie, A.V., Carroll, P.L., et al. (2023). In silico protein interaction screening uncovers DONSON's role in replication initiation. Science *381*, eadi3448. doi:10.1126/science.adi3448.
Liu, Y., Qin, S., Lei, M., Tempel, W., Zhang, Y., Loppnau, P., Li, Y., and Min, J. (2017). Peptide recognition by heterochromatin protein 1 (HP1) chromoshadow domains revisited: Plasticity in the pseudosymmetric histone binding site of human HP1. J Biol Chem *292*, 5655-5664. 10.1074/jbc.M116.768374.
Lu, R., and Wang, G.G. (2013). Tudor: a versatile family of histone methylation 'readers'. Trends Biochem Sci *38*, 546-555. 10.1016/j.tibs.2013.08.002.
Mendez, D.L., Kim, D., Chruszcz, M., Stephens, G.E., Minor, W., Khorasanizadeh, S., and Elgin, S.C. (2011). The HP1a disordered C terminus and chromo shadow domain cooperate to select target peptide partners. Chembiochem *12*, 1084-1096. 10.1002/cbic.201000598.
Mendez, D.L., Mandt, R.E., and Elgin, S.C.R. (2013). Heterochromatin Protein 1a (HP1a) Partner Specificity Is Determined by Critical Amino Acids in the Chromo Shadow Domain and C-terminal Extension *. Journal of Biological Chemistry *288*, 22315-22323. 10.1074/jbc.M113.468413.
Misteli, T. (2020). The Self-Organizing Genome: Principles of Genome Architecture and Function. Cell *183*, 28-45. 10.1016/j.cell.2020.09.014.
Moazed, D. (2011). Mechanisms for the inheritance of chromatin states. Cell *146*, 510-518. 10.1016/j.cell.2011.07.013.
Motamedi, M.R., Hong, E.-J.E., Li, X., Gerber, S., Denison, C., Gygi, S., and Moazed, D. (2008). HP1 Proteins Form Distinct Complexes and Mediate Heterochromatic Gene Silencing by Nonoverlapping Mechanisms. Molecular Cell *32*, 778-790. 10.1016/j.molcel.2008.10.026.
Munkres, J. (1957). Algorithms for the Assignment and Transportation Problems. Journal of the Society for Industrial and Applied Mathematics *5*, 32-38. 10.1137/0105003.
Nakayama, J.-i., Klar, A.J.S., and Grewal, S.I.S. (2000). A Chromodomain Protein, Swi6, Performs Imprinting Functions in Fission Yeast during Mitosis and Meiosis. Cell *101*, 307-317. 10.1016/S0092-8674(00)80840-5.
Petryk, N., Dalby, M., Wenger, A., Stromme, C.B., Strandsby, A., Andersson, R., and Groth, A. (2018). MCM2 promotes symmetric inheritance of modified histones during DNA replication. Science *361*, 1389-1392. 10.1126/science.aau0294.
Pettersen, E.F., Goddard, T.D., Huang, C.C., Couch, G.S., Greenblatt, D.M., Meng, E.C., and Ferrin, T.E. (2004). UCSF Chimera--a visualization system for exploratory research and analysis. J Comput Chem *25*, 1605-1612. 10.1002/jcc.20084.
Ragunathan, K., Jih, G., and Moazed, D. (2015). Epigenetic inheritance uncoupled from sequence-specific recruitment. Science *348*, 1258699. doi:10.1126/science.1258699.
Raiymbek, G., An, S., Khurana, N., Gopinath, S., Larkin, A., Biswas, S., Trievel, R.C., Cho, U.-s., and Ragunathan, K. (2020). An H3K9 methylation-dependent protein interaction regulates the non-enzymatic functions of a putative histone demethylase. eLife *9*, e53155. 10.7554/eLife.53155.

Ramírez, F., Ryan, D.P., Grüning, B., Bhardwaj, V., Kilpert, F., Richter, A.S., Heyne, S., Dündar, F., and Manke, T. (2016). deepTools2: a next generation web server for deep-sequencing data analysis. Nucleic Acids Research *44*, W160-W165. 10.1093/nar/gkw257.
Rea, S., Eisenhaber, F., O'Carroll, D., Strahl, B.D., Sun, Z.W., Schmid, M., Opravil, S., Mechtler, K., Ponting, C.P., Allis, C.D., and Jenuwein, T. (2000). Regulation of chromatin structure by site-specific histone H3 methyltransferases. Nature *406*, 593-599. 10.1038/35020506.
Reinberg, D., and Vales, L.D. (2018). Chromatin domains rich in inheritance. Science *361*, 33-34. 10.1126/science.aat7871.
Ringrose, L., Ehret, H., and Paro, R. (2004). Distinct contributions of histone H3 lysine 9 and 27 methylation to locus-specific stability of polycomb complexes. Mol Cell *16*, 641-653. 10.1016/j.molcel.2004.10.015.
Roche, B., Arcangioli, B., and Martienssen, R.A. (2016). RNA interference is essential for cellular quiescence. Science *354*. 10.1126/science.aah5651.
Rougemaille, M., Braun, S., Coyle, S., Dumesic, P.A., Garcia, J.F., Isaac, R.S., Libri, D., Narlikar, G.J., and Madhani, H.D. (2012). Ers1 links HP1 to RNAi. Proceedings of the National Academy of Sciences *109*, 11258-11263. 10.1073/pnas.1204947109.
Rowland, D.J., and Biteen, J.S. (2017). Measuring molecular motions inside single cells with improved analysis of single-particle trajectories. Chemical Physics Letters *674*, 173-178.
Sadaie, M., Kawaguchi, R., Ohtani, Y., Arisaka, F., Tanaka, K., Shirahige, K., and Nakayama, J.-i. (2008). Balance between Distinct HP1 Family Proteins Controls Heterochromatin Assembly in Fission Yeast. Molecular and Cellular Biology *28*, 6973-6988. 10.1128/MCB.00791-08.
Sadaie, M., Kawaguchi, R., Ohtani, Y., Arisaka, F., Tanaka, K., Shirahige, K., and Nakayama, J.-i. (2023). Balance between Distinct HP1 Family Proteins Controls Heterochromatin Assembly in Fission Yeast. Molecular and Cellular Biology *28*, 6973-6988. 10.1128/mcb.00791-08.
Sanchez, R., and Zhou, M.M. (2011). The PHD finger: a versatile epigenome reader. Trends Biochem Sci *36*, 364-372. 10.1016/j.tibs.2011.03.005.
Sanulli, S., Trnka, M.J., Dharmarajan, V., Tibble, R.W., Pascal, B.D., Burlingame, A.L., Griffin, P.R., Gross, J.D., and Narlikar, G.J. (2019). HP1 reshapes nucleosome core to promote phase separation of heterochromatin. Nature *575*, 390-394. 10.1038/s41586-019-1669-2.
Seman, M., Levashkevich, A., Larkin, A., Huang, F., and Ragunathan, K. (2023). Uncoupling the distinct functions of HP1 proteins during heterochromatin establishment and maintenance. Cell Reports *42*. 10.1016/j.celrep.2023.113428.
Shan, C.-M., Bao, K., Diedrich, J., Chen, X., Lu, C., Yates, J.R., and Jia, S. (2020). The INO80 Complex Regulates Epigenetic Inheritance of Heterochromatin. Cell Reports *33*, 108561. https://doi.org/10.1016/j.celrep.2020.108561.
Shimada, A., Dohke, K., Sadaie, M., Shinmyozu, K., Nakayama, J.-I., Urano, T., and Murakami, Y. (2009). Phosphorylation of Swi6/HP1 regulates transcriptional gene silencing at heterochromatin. Genes & Development *23*, 18-23. 10.1101/gad.1708009.
Shipkovenska, G., Durango, A., Kalocsay, M., Gygi, S.P., and Moazed, D. (2020). A conserved RNA degradation complex required for spreading and epigenetic inheritance of heterochromatin. Elife *9*. 10.7554/eLife.54341.
Smothers, J.F., and Henikoff, S. (2000). The HP1 chromo shadow domain binds a consensus peptide pentamer. Curr Biol *10*, 27-30. 10.1016/s0960-9822(99)00260-2.
Soltermann, F., Foley, E.D.B., Pagnoni, V., Galpin, M., Benesch, J.L.P., Kukura, P., and Struwe, W.B. (2020). Quantifying Protein-Protein Interactions by Molecular Counting with Mass Photometry. Angew Chem Int Ed Engl *59*, 10774-10779. 10.1002/anie.202001578.
Stephens, G.E., Slawson, E.E., Craig, C.A., and Elgin, S.C. (2005). Interaction of heterochromatin protein 2 with HP1 defines a novel HP1-binding domain. Biochemistry *44*, 13394-13403. 10.1021/bi051006+.
Stewart-Morgan, K.R., Petryk, N., and Groth, A. (2020). Chromatin replication and epigenetic cell memory. Nature Cell Biology *22*, 361-371. 10.1038/s41556-020-0487-y.

Strahl, B.D., and Allis, C.D. (2000). The language of covalent histone modifications. Nature *403*, 41-45. 10.1038/47412.
Strom, A.R., Emelyanov, A.V., Mir, M., Fyodorov, D.V., Darzacq, X., and Karpen, G.H. (2017). Phase separation drives heterochromatin domain formation. Nature *547*, 241-245. 10.1038/nature22989.
Takahata, S., Chida, S., Ohnuma, A., Ando, M., Asanuma, T., and Murakami, Y. (2021). Two secured FACT recruitment mechanisms are essential for heterochromatin maintenance. Cell Reports *36*, 109540. https://doi.org/10.1016/j.celrep.2021.109540.
Thiru, A., Nietlispach, D., Mott, H.R., Okuwaki, M., Lyon, D., Nielsen, P.R., Hirshberg, M., Verreault, A., Murzina, N.V., and Laue, E.D. (2004). Structural basis of HP1/PXVXL motif peptide interactions and HP1 localisation to heterochromatin. Embo j *23*, 489-499. 10.1038/sj.emboj.7600088.
Thon, G., and Verhein-Hansen, J. (2000). Four Chromo-domain Proteins of Schizosaccharomyces pombe Differentially Repress Transcription at Various Chromosomal Locations. Genetics *155*, 551-568. 10.1093/genetics/155.2.551.
Torres-Garcia, S., Di Pompeo, L., Eivers, L., Gaborieau, B., White, S.A., Pidoux, A.L., Kanigowska, P., Yaseen, I., Cai, Y., and Allshire, R.C. (2020a). SpEDIT: A fast and efficient CRISPR/Cas9 method for fission yeast. Wellcome Open Res *5*, 274. 10.12688/wellcomeopenres.16405.1.
Torres-Garcia, S., Yaseen, I., Shukla, M., Audergon, P., White, S.A., Pidoux, A.L., and Allshire, R.C. (2020b). Epigenetic gene silencing by heterochromatin primes fungal resistance. Nature *585*, 453-458. 10.1038/s41586-020-2706-x.
Trewick, S.C., McLaughlin, P.J., and Allshire, R.C. (2005). Methylation: lost in hydroxylation? EMBO Rep *6*, 315-320. 10.1038/sj.embor.7400379.
Trewick, S.C., Minc, E., Antonelli, R., Urano, T., and Allshire, R.C. (2007). The JmjC domain protein Epe1 prevents unregulated assembly and disassembly of heterochromatin. Embo j *26*, 4670-4682. 10.1038/sj.emboj.7601892.
Uckelmann, M., and Davidovich, C. (2021). Not just a writer: PRC2 as a chromatin reader. Biochem Soc Trans *49*, 1159-1170. 10.1042/bst20200728.
Vakoc, C.R., Mandat, S.A., Olenchock, B.A., and Blobel, G.A. (2005). Histone H3 lysine 9 methylation and HP1gamma are associated with transcription elongation through mammalian chromatin. Mol Cell *19*, 381-391. 10.1016/j.molcel.2005.06.011.
Wang, J., Tadeo, X., Hou, H., Tu, P.G., Thompson, J., Yates, J.R., and Jia, S. (2013). Epe1 recruits BET family bromodomain protein Bdf2 to establish heterochromatin boundaries. Genes & Development *27*, 1886-1902. 10.1101/gad.221010.113.
Xu, M., Long, C., Chen, X., Huang, C., Chen, S., and Zhu, B. (2010). Partitioning of Histone H3-H4 Tetramers During DNA Replication–Dependent Chromatin Assembly. Science *328*, 94-98. 10.1126/science.1178994.
Yamada, T., Fischle, W., Sugiyama, T., Allis, C.D., and Grewal, S.I.S. (2005). The Nucleation and Maintenance of Heterochromatin by a Histone Deacetylase in Fission Yeast. Molecular Cell *20*, 173-185. 10.1016/j.molcel.2005.10.002.
Yamada, T., Fukuda, R., Himeno, M., and Sugimoto, K. (1999). Functional domain structure of human heterochromatin protein HP1(Hsalpha): involvement of internal DNA-binding and C-terminal self-association domains in the formation of discrete dots in interphase nuclei. J Biochem *125*, 832-837. 10.1093/oxfordjournals.jbchem.a022356.
Yamagishi, Y., Sakuno, T., Shimura, M., and Watanabe, Y. (2008). Heterochromatin links to centromeric protection by recruiting shugoshin. Nature *455*, 251-255. 10.1038/nature07217.
Yaseen, I., White, S.A., Torres-Garcia, S., Spanos, C., Lafos, M., Gaberdiel, E., Yeboah, R., El Karoui, M., Rappsilber, J., Pidoux, A.L., and Allshire, R.C. (2022). Proteasome-dependent truncation of the negative heterochromatin regulator Epe1 mediates antifungal resistance. Nat Struct Mol Biol *29*, 745-758. 10.1038/s41594-022-00801-y.

Yu, C., Gan, H., Serra-Cardona, A., Zhang, L., Gan, S., Sharma, S., Johansson, E., Chabes, A., Xu, R.-M., and Zhang, Z. (2018). A mechanism for preventing asymmetric histone segregation onto replicating DNA strands. Science *361*, 1386-1389. 10.1126/science.aat8849.

Yun, M., Wu, J., Workman, J.L., and Li, B. (2011). Readers of histone modifications. Cell Res *21*, 564-578. 10.1038/cr.2011.42.

Zhang, H., Qin, W., Romero, H., Leonhardt, H., and Cardoso, M.C. (2023). Heterochromatin organization and phase separation. Nucleus *14*, 2159142. 10.1080/19491034.2022.2159142.

Zhang, K., Mosch, K., Fischle, W., and Grewal, S.I. (2008a). Roles of the Clr4 methyltransferase complex in nucleation, spreading and maintenance of heterochromatin. Nat Struct Mol Biol *15*, 381-388. 10.1038/nsmb.1406.

Zhang, L., and Elias, J.E. (2017). Relative Protein Quantification Using Tandem Mass Tag Mass Spectrometry. Methods Mol Biol *1550*, 185-198. 10.1007/978-1-4939-6747-6_14.

Zhang, Y., Liu, T., Meyer, C.A., Eeckhoute, J., Johnson, D.S., Bernstein, B.E., Nusbaum, C., Myers, R.M., Brown, M., Li, W., and Liu, X.S. (2008b). Model-based Analysis of ChIP-Seq (MACS). Genome Biology *9*, R137. 10.1186/gb-2008-9-9-r137.

Zofall, M., and Grewal, S.I.S. (2006). Swi6/HP1 Recruits a JmjC Domain Protein to Facilitate Transcription of Heterochromatic Repeats. Molecular Cell *22*, 681-692. 10.1016/j.molcel.2006.05.010.

Zofall, M., Sandhu, R., Holla, S., Wheeler, D., Grewal, S.I.S. (2022). Histone deacetylation primes self-propagation of heterochromatin domains to promote epigenetic inheritance. Nature Structural & Molecular Biology *29*, 898–909. https://doi.org/10.1038/s41594-022-00830-7.